


## RESEARCH ARTICLE

# Characterization of cortical hemodynamic changes following sensory, visual, and speech activation by intraoperative optical imaging utilizing phase-based evaluation methods

Martin Oelschlägel<sup>1</sup>  | Witold H. Polanski<sup>2</sup> | Ute Morgenstern<sup>3</sup> | Gerald Steiner<sup>1</sup> | Matthias Kirsch<sup>2,4</sup> | Edmund Koch<sup>1</sup> | Gabriele Schackert<sup>2</sup> | Stephan B. Sobottka<sup>2</sup>

<sup>1</sup>Department of Anesthesiology and Intensive Care Medicine, Technische Universität Dresden, Carl Gustav Carus Faculty of Medicine, Clinical Sensing and Monitoring, Dresden, Saxony, Germany

<sup>2</sup>Department of Neurosurgery, Technische Universität Dresden, Carl Gustav Carus University Hospital Dresden, Dresden, Saxony, Germany

<sup>3</sup>Faculty of Electrical and Computer Engineering, Technische Universität Dresden, Institute of Biomedical Engineering, Dresden, Saxony, Germany

<sup>4</sup>Department of Neurosurgery, Asklepios Kliniken Schildautal Seesen, Seesen, Saxony, Germany

## Correspondence

Martin Oelschlägel, Technische Universität Dresden, Medizinische Fakultät Carl Gustav Carus, Klinisches Sensing und Monitoring, Fetscherstraße 74, 01307 Dresden, Saxony, Germany.  
Email: martin.oelschlaegel@tu-dresden.de

## Funding information

Martin Oelschlägel received PhD funding from Carl Zeiss Meditec AG, Oberkochen, Germany. Additionally, material support (camera systems, optical components) was provided by Carl Zeiss Meditec AG.

## Abstract

Alterations within cerebral hemodynamics are the intrinsic signal source for a wide variety of neuroimaging techniques. Stimulation of specific functions leads due to neurovascular coupling, to changes in regional cerebral blood flow, oxygenation and volume. In this study, we investigated the temporal characteristics of cortical hemodynamic responses following electrical, tactile, visual, and speech activation for different stimulation paradigms using Intraoperative Optical Imaging (IOI). Image datasets from a total of 22 patients that underwent surgical resection of brain tumors were evaluated. The measured reflectance changes at different light wavelength bands, representing alterations in regional cortical blood volume (CBV), and deoxyhemoglobin (HbR) concentration, were assessed by using Fourier-based evaluation methods. We found a decrease of CBV connected to an increase of HbR within the contralateral primary sensory cortex (SI) in patients that were prolonged (30 s/15 s) electrically stimulated. Additionally, we found differences in amplitude as well as localization of activated areas for different stimulation patterns. Contrary to electrical stimulation, prolonged tactile as well as prolonged visual stimulation are provoking increases in CBV within the corresponding activated areas (SI, visual cortex). The processing of the acquired data from awake patients performing speech tasks reveals areas with increased, as well as areas with decreased CBV. The results lead us to the conclusion, that the CBV decreases in connection with HbR increases

**Abbreviations:** AAM, activity amplitude map (two-dimensional);  $\bar{A}_{\text{TRep}}$ , mean activity level within trepanation obtained from activity amplitude map; AU, arbitrary units; BOLD, blood oxygen level dependent; CBV, cerebral blood volume; CCD, charge coupled device; CMOS, complementary metal-oxide-semiconductor; DCS, direct cortical stimulation; FFT, fast Fourier transform; FIR, finite impulse response (Filter); fMRI, functional magnetic resonance imaging; fNIRS, functional near infrared spectroscopy;  $f_{\text{SNE}}$ , stimulation frequency of electrical median nerve stimulation;  $f_{\text{SNV}}$ , stimulation frequency of visual stimulation (flash frequency); fUS, functional ultrasound; FWHM, full width at half maximum; HbO, oxygenated hemoglobin; HbR, reduced hemoglobin; HSV, Hue saturation value (color space/color planes); IOIS/IOI, optical imaging of intrinsic signals/intraoperative optical imaging; ITK, insight segmentation and registration toolkit; N/A, not applicable;  $n_{\text{actSI}}$ , number of active pixels within SI area;  $n_{\text{actSurr}}$ , number of active pixels within surrounding area; NBR, negative BOLD response;  $n_{\text{SI}}$ , number of total pixels of SI area;  $n_{\text{surr}}$ , number of total pixels of surrounding area; PAD, phase angle distribution (polar histogram); PAM, phase angle map (two-dimensional); PBR, positive BOLD response;  $P_s$ , power spectral density map of stimulation component; PSD, power spectral density;  $P_{\text{Vif}}$ , power spectral density map of very-low-frequency band; RGB, red green blue (color space/color planes/color channels of camera); S, scaling factor;  $S_{\text{TRep}}$ , standard deviation of activity level within trepanation obtained from activity amplitude map; SI, primary sensory cortex (SI Area); SNR, signal-to-noise ratio; SPECT, single photon emission computed tomography;  $V_x$ , time series data cube (X, Y, time) after different processing steps;  $z_{\text{Thresh}}$ , threshold for segmentation of amplitude activity map;  $\sigma$ , Kernel size of Gaussian filter.

This is an open access article under the terms of the Creative Commons Attribution-NonCommercial-NoDerivs License, which permits use and distribution in any medium, provided the original work is properly cited, the use is non-commercial and no modifications or adaptations are made.

© 2021 The Authors. *Human Brain Mapping* published by Wiley Periodicals LLC.

in SI are associated to processing of nociceptive stimuli and that stimulation type, as well as paradigm have a nonnegligible impact on the temporal characteristics of the following hemodynamic response.

#### KEYWORDS

cortical hemodynamics, intraoperative optical imaging, nociceptive stimuli, speech activation, tactile stimulation, visual

## 1 | INTRODUCTION

Functional imaging of the human brain is continuously increasing our understanding for neuronal connectivity and cognitive processing in health as well as in disease (Hadjiabadi et al., 2018; Mikdashi, 2016; van den Heuvel & Pol, 2010). Hemodynamic changes following neuronal activation due to neurovascular coupling are hereby the most important intrinsic signal source for a wide variety of different neuroimaging methods including functional Near-Infrared Spectroscopy (fNIRS) (Arenth, Ricker, & Schultheis, 2007; Ferrari, Mottola, & Quaresima, 2004; Villringer, Planck, Hock, Schleinkofer, & Dirnagl, 1993), functional Ultrasound Imaging (fUS) (Mace et al., 2013; Macé et al., 2011), Optical Imaging of Intrinsic Signals/Intraoperative Optical Imaging (iOIS/IOI) (Haglund, Ojemann, & Hochman, 1992; Morone, Neimat, Roe, & Friedman, 2017; Pouratian, Cannestra, Martin, & Toga, 2002a), and probably most importantly functional Magnetic Resonance Imaging (fMRI) (Ances et al., 2008; Huppert, Allen, Diamond, & Boas, 2009; Sotero & Trujillo-Barreto, 2008). Beyond the pursuit of gaining knowledge about structural and functional relationships, the use of the different techniques is essential for patients undergoing surgical treatment of pathological brain processes like tumors (Castellano, Cirillo, Bello, Riva, & Falini, 2017; Kapsalakis et al., 2012; Silva, See, Essayed, Golby, & Tie, 2018). Here, the main scope is the preservation of essential functional areas while maximizing the extent of tumor tissue resection (Sanai & Berger, 2008; Senft et al., 2011; Stummer et al., 2008). Therefore, an exact localization of the functional areas is mandatory. In recent years, our group evolved IOI towards a clinical tool that can be easily and intraoperatively applied for a wide variety of use cases including the visualization of language, motor, visual, and sensory processing areas (Oelschlägel et al., 2018–2020; Sobottka et al., 2013a–2013b). The stimulation and evaluation methodology comprised a periodic stimulation paradigm in connection with fast Fourier-based image processing (Oelschlägel et al., 2013). Although the above-mentioned imaging techniques, including our own IOI, are widely applied, there is evidence, that different stimulation patterns, stimulation types, and stimulation sites as well as the local vascular structure and pathological processes have a nonnegligible impact on the induced hemodynamic changes and therefore on the results and reliability of the different modalities (Backes, Mess, van Kranen-Mastenbroek, & Reulen, 2000; Parkes, Fries, Kerskens, & Norris, 2004; Robinson et al., 2006). Especially in respect to nociceptive stimuli, studies have shown that those might trigger local deactivation or inhibition of the corresponding brain areas and therefore a different

hemodynamic response than activations following nonnociceptive stimuli (Apkarian et al., 1992; Disbrow, Buonocore, Antognini, Carstens, & Rowley, 1998). In connection with this phenomenon, there is ongoing discussion about the role of the universally observed negative Blood-Oxygenation-Level-Dependent (BOLD) response in fMRI (Tal, Geva, & Amedi, 2017; Wilson, Thomas, & Mayhew, 2020). It is interpreted most commonly as neuronal deactivation or inhibition (Stefanovic, Warnking, & Pike, 2004; Sten et al., 2017), but some studies are revealing a more complex situation since different hemodynamic mechanisms at various depth layers of the brain might be the trigger for the positive BOLD response (PBR) and the negative BOLD response (NBR) (Goense, Merkle, & Logothetis, 2012; Huber et al., 2014; Mullinger, Mayhew, Bagshaw, Bowtell, & Francis, 2014).

The main scope of this study is shedding light on hemodynamic changes, namely changes in cerebral blood volume ( $\Delta$ CBV) and changes in deoxyhemoglobin ( $\Delta$ HbR), from IOI perspective for different stimuli as well as different stimulation patterns. We extended our evaluation methodology that initially was developed to identify functional brain areas based on the amplitude information of the signal, by computing and visualizing now additionally the phase angle information of the measured signals. The results of this modification are two-dimensional maps of relative  $\Delta$ CBV and  $\Delta$ HbR, whereas it is known that the  $\Delta$ HbR signal and the fMRI BOLD response share the same etiology, although the IOI signal at this wavelength may also contain smaller components arising from other sources (Pouratian et al., 2002b; Prakash et al., 2009). With the optimized phase-resolved IOI, we pooled retrospectively a highly diversified patient cohort from our database and evaluated the hemodynamic responses towards different stimulations patterns of electrical stimulation as well as the hemodynamic responses following tactile, visual, and speech stimulation. This should on the one hand increase the general understanding of activations following different stimuli types (e.g., nociceptive and non-nociceptive stimuli), and on the other hand the results can be used for the optimization of IOI as well as other imaging modalities that rely on periodic stimuli and the subsequent hemodynamic response.

## 2 | MATERIALS AND METHODS

### 2.1 | Intraoperative optical imaging

Minimal changes in the cortical optical properties of the brain surface are the intrinsic signal source for the IOI technique. The optical signal

is induced by functional hyperemia after neuronal activation and can be detected as a change in reflectance signal (change in absorption of tissue), measured with highly sensitive Charge-Coupled-Device (CCD) or Complementary Metal-Oxide-Semiconductor (CMOS) camera systems directly from the exposed cortical surface during surgery. The signal is most commonly described as either monophasic (CBV, total hemoglobin [HbT] signal) or biphasic (HbR signal). For a single stimulation event of short duration ( $\sim 1\text{--}2$  s), the CBV signal is estimated to reach its peak value within 3–5 s after stimulation end, whereas the first maximum of the HbR response (early phase) can be observed after 0.5–1.5 s poststimulation. The second peak of the HbR signal is reached, like the CBV response, within 3–5 s (Morone et al., 2017; Prakash et al., 2009). Due to the light wavelength dependent absorption characteristics of HbR and HbO, reflectance measure within a range from  $\lambda = 500\text{--}599$  nm (and especially on isosbestic points within this range) is dominated by changes of CBV (HbT), whereas the signal acquired within a range from  $\lambda = 600\text{--}699$  nm is highly associated to changes in HbR (Morone et al., 2017). The signals that are following short stimulation events are well described with IOI in human as well as in animal models, but longer lasting and repetitive stimulations and the subsequent hemodynamic response are little investigated with this technique, especially in humans. The most widely used method of data acquisition and analysis of IOI signals is based on a relative differences approach, where a measured reflectance change after stimulation  $\Delta R$  is calculated in relation to the reflectance  $R$  during a baseline condition (Cannestra et al., 2001; Sato et al., 2002 2005; Suh, Bahar, Mehta, & Schwartz, 2006). Areas that are showing an increased  $\Delta R/R$  ratio after stimulation are usually interpreted as activated, respectively, responding to the stimulus. Since this approach is very susceptible for any kind of unwanted change in reflection (arising specular reflections due to desiccation of cortical surface, movement etc.), our group is using a Fourier-based approach of data evaluation in connection with periodic repetition of stimulation. Subsequently, we are describing the patient characteristics, stimulation protocols, and image acquisition procedures, followed by a detailed explanation of the evaluation methodology.

## 2.2 | Patients and stimulation protocol

Image sequences from a total of 22 patients (11 female, 11 male, median age 57.5 years) with different patterns and stimulation types were pooled from our existing database and re-evaluated in respect to the signal phase angle of the stimulation frequency  $f_{stim}$ . The patient characteristics are shown in Table 1. Electrical stimulation of the median nerve was performed in 15 patients, three patients were tactile irritated on the hand, three patients were visually stimulated using flashlight goggles for visual evoked potentials (VEP), and three patients performed speech tasks during awake surgery. In summary, a total of 28 stimulations were evaluated, the assignment between stimulation type, pattern, and patients is also given in Table 1. Electrical and tactile stimulations were performed on the median nerve/hand contralateral to craniotomized side. For the electrical stimulation,

standard neurostimulation devices were used (Bravo Endeavor, Nicolet Biomedical, WI or ISIS, Inomed, Emmendingen, Germany) applying a stimulation current amplitude of  $I_{stim} = 20$  mA with stimulation frequencies of  $f_{SNE} = 4.7$  Hz or 5.1 Hz (pulse duration = 200/300  $\mu$ s). The visual stimulation frequency was  $f_{SNV} = 1.1$  Hz or 3.1 Hz (flash duration = 5 ms), stimulating both eyes. Stimulation frequencies were chosen according to electrophysiological recommendations for clinical standard procedures. Tactile irritation was done by applying a surgical rubber manually on the palm and dorsum of the hand located also contralateral to craniotomized side. Electrical, tactile, and visual stimulation were performed whilst patients were under general anesthesia. Speech paradigm under local anesthesia consisted of overt verbalization from visually presented objects. The objects were presented using timed slides on a screen attached within the visual field of the patient. During the rest trials, blank slides were shown. Additional information and results of this approach compared to fMRI is also available in Oelschlägel et al. (2020). The stimulations of all different types (electrical, tactile, visual, and speech) were applied repetitive in block designs and each sequence started with a rest trial. Rest and stimulation trials were of equal length, either both 30 s ([30R – 30S] design) or both 15 s ([15R – 15S] design).

## 2.3 | Image acquisition, patient characteristics, and stimulation protocols

Image acquisition was performed using optical imaging camera systems attached via beam splitter to the surgical microscope (hardware-setup #1, #2, #4, Table 2) or by using simply the microscope integrated RGB camera for recording of the video sequences (hardware-setup #3). Wavelength filtering was performed within optical path, in case a monochrome camera system was used. A detailed overview over the components of each system is given in Table 2. The assignment of each system to the patients is shown in Table 1. Recording of image data was performed over 270 s (nine trials, 15 s rest, 15 s stimulation) or 540 s (nine trials, 30 s rest, 30 s stimulation). Images were acquired with 4–50 frames per second using exposure times of 1 ms (hardware-setup #2), 50 ms (hardware-setup #1), or 700–800 ms (hardware-setup #4). The exposure time for image data recorded with hardware-setup #3 was automatically adjusted by the microscope. Here, illumination was set to 20% of the maximum intensity available to achieve a visually well-illuminated scene. Temporal down sampling and equidistant timecourse interpolation (linear) was performed for image data of all setups, targeting at a framerate of four frames per second for data evaluation. Images acquired with the narrowband 568 nm (FWHM = 10 nm) filter are due to the same absorption coefficient of deoxy- and oxyhemoglobin at this wavelength (isosbestic point) representative maps of  $\Delta$ CBV (Ma et al., 2016) whereas image data acquired at a central wavelength of 600 nm, respectively, within the spectral sensitivity of the red channel (RGB camera, red channel peak sensitivity  $\sim 600$  nm, FWHM  $\sim 50$  nm), are maps of  $\Delta$ HbR that correlate with the fMRI BOLD response (Pouratian, Sicotte, et al., 2002b; Prakash et al., 2009).

**TABLE 1** Patient characteristics and stimulation protocols

Patient no.	Age	Sex	Histopathology	Tumor localization (hemisphere, lobe)	Stimulation (type, protocol, site)	Hardware setup no.	Wavelength/physiological component
#1	58	F	Meningioma	Left, parietal	Electrical, [30R – 30S], median nerve	#1	568 nm/CBV
#2	78	M	Metastasis (bronchial carcinoma)	Left, parietal	Electrical, [30R – 30S], [15R – 15S], median nerve	#1	568 nm/CBV
#3	54	F	Meningioma	Right, parietal and left frontal	Electrical, [30R – 30S], [15R – 15S], median nerve	#1	568 nm & 600 nm/CBV & HbR
#4	66	M	Anaplastic astrocytoma	Right, frontal	Electrical, [30R – 30S], [15R – 15S], median nerve	#1	568 nm/CBV
#5	68	F	Glioblastoma	Right, temporal/parietal	Electrical, [30R – 30S], [15R – 15S], median nerve	#1	568 nm/CBV
#6	33	F	Metastasis (mammary carcinoma)	Left, parietal	Electrical, [30R – 30S], [15R – 15S], median nerve	#1	568 nm/CBV
#7	50	F	Metastasis (melanoma)	Left, parietal & right temporal/parietal	Electrical, [30R – 30S], median nerve	#1	568 nm/CBV
#8	54	M	Glioblastoma (multifocal)	Left, parietal/occipital	Electrical, [30R – 30S], median nerve	#3	RGB (Red Channel)/HbR
#9	65	M	Glioblastoma	Left, frontal/parietal	Electrical, [15R – 15S], median nerve	#1	568 nm/CBV
#10	58	F	Oligoastro-cytoma	Right, frontal	Electrical, [30R – 30S], median nerve	#2	RGB (Red Channel)/HbR
#11	25	F	Glioblastoma	Right, frontal	Electrical, [30R – 30S], median nerve	#2	RGB (Red Channel)/HbR
#12	68	M	Gliosarcoma	Left, parietal	Electrical, [30R – 30S], median nerve	#2	RGB (Red Channel)/HbR
#13	72	M	Anaplastic oligo-dendroglioma	Right, parietal	Electrical, [30R – 30S], median nerve	#3	RGB (Red Channel)/HbR
#14	81	M	Metastasis (melanoma)	Left, parietal	Tactile/electrical, [30R – 30S], hand/ median nerve	#1	568 nm/CBV
#15	32	F	Meningioma	Left, parietal	Tactile/electrical, [30R – 30S], hand/median nerve	#1	568 nm/CBV
#16	78	F	Metastasis (bronchial carcinoma)	Left, parietal	Tactile, [30R – 30S], hand	#1	568 nm/CBV
#17	57	F	Metastasis (mammary carcinoma)	Right, occipital	Visual, [30R – 30S], eyes	#1	568 nm/CBV
#18	74	M	Astrocytoma	Right, occipital	Visual, [30R – 30S], eyes	#4	568 nm/CBV
#19	37	F	Cavernoma	Right, occipital	Visual, [30R – 30S], eyes	#1	568 nm/CBV
#20	41	M	Astrocytoma	Left, insular	Speech, [30R – 30S], N/A	#4	568 nm/CBV
#21	34	M	Oligoastrocytoma	Left, temporal/insular	Speech, [30R – 30S], N/A	#1	568 nm/CBV
#22	36	M	Astrocytoma	Left, frontal/temporal	Speech, [30R – 30S], N/A	#1	568 nm/CBV

Note: Abbreviations for stimulation protocols are as follows: [30R – 30S] = 30 s rest trial, 30 s stimulation trial (duration of continuous stimulation), [15R – 15S] analogous with changed duration of the rest and stimulation trials.

## 2.4 | Calculation of activity amplitude maps and phase angle maps

In the initial evaluation step, image sequences were corrected for motion artifacts using a nonrigid image registration based on Demon's algorithm (Thirion, 1998). The Amplitude Activity Maps (AAM) were

then calculated from motion corrected video (time series) data of the exposed cortical surface of the patients, by performing a fast Fourier transform for each pixel with subsequent Power Spectral Density (PSD) calculation. Prior to transform, acquired time courses of each pixel were interpolated (linear) to equidistant sample points to correct for little variations in sampling rate during acquisition. Since different

**TABLE 2** Imaging Hardware used for data acquisition

Hardware-setup no.	Camera	Filter	Microscope	Illumination	Spatial resolution (number of pixels)	Temporal resolution (fps)
#1	AxioCam MRm (Carl Zeiss MicroImaging, Jena, Germany)	Bandpass interference filter, central wavelength $\lambda_C = 568$ nm, FWHM = 10 nm or $\lambda_C = 600$ nm (Edmund optics, Barrington NJ)	OPMI Pico (Carl Zeiss Meditec AG, Oberkochen, Germany)	180 W xenon (microscope integrated)	$692 \times 520$ ( $2 \times 2$ binning mode)	4–15
#2	Trio 620 (Carl Zeiss Meditec AG, Oberkochen, Germany)	No additional (red channel spectral response, 3-Chip-CCD camera)	OPMI Pentero/Pentero 900 (Carl Zeiss Meditec AG, Oberkochen, Germany)	300 W xenon (microscope integrated)	$1920 \times 1080$	7
#3	Microscope integrated	No additional (red channel spectral response, 3-Chip-CCD camera)	Kinevo 900 (Carl Zeiss Meditec AG, Oberkochen, Germany)	300 W xenon (microscope integrated)	$1920 \times 1080$	50
#4	Hamamatsu C4742-96-12G04 (Hamamatsu photonics, Hamamatsu, Japan)	Bandpass interference filter, central wavelength $\lambda_C = 568$ nm, FWHM = 10 nm (Edmund optics, Barrington NJ)	VM-900 (Möller-wedel, wedel, Germany)	150 W halogen (stabilized)	$672 \times 512$	7

imaging systems were used for data acquisition, down-sampling to 4 Hz was performed for all datasets, as this was the lowest frame rate used during image acquisition (see Table 2, setup #1). To compensate for slow drifts over the duration of the image acquisition process (e.g., from illumination and desiccation of the cortical surface), and to remove the constant component in frequency domain, the time courses were additionally corrected by fitting and subtracting a cubic polynomial. After PSD calculation, a two-dimensional map ( $P_s$ ) was calculated, in which each pixel value corresponds to the PSD value of the stimulation frequency component. Therefore, peak value from PSD exactly at stimulation frequency was used (see Figure 1). Due to selected framerate of 4 Hz (sample rate) and recording duration (540 s/270 s), stimulation frequencies are discrete points on the PSD frequency axis for the investigated stimulation patterns ( $f_{stim} = 1/60$  s = 0.0167 Hz or  $f_{stim} = 1/30$  s = 0.0334 Hz). Additionally, a second two-dimensional map was calculated ( $P_{VLF}$ ), where each pixel value corresponds to the sum of the PSD within the very-low frequency vasomotion band ( $f < 0.04$  Hz). Finally, the ratio of both two-dimensional maps was calculated (pixel-by-pixel division), resulting in the AAM (“PSD ratio activity map”, see Figure 1c), which visualizes reliably the cortical region, that is activated by the stimulation (e.g., the median nerve area on the primary sensory cortex SI [Oelschlägel et al., 2013; Sobottka, Meyer, Kirsch, Koch, et al., 2013a]).

During fast Fourier transform, we discarded the phase information in previous studies and used only the amplitude information (AAM) to localize the functional areas (Meyer et al., 2013; Oelschlägel et al., 2013; Sobottka, Meyer, Kirsch, Koch, et al., 2013a). To investigate the direction and the temporal characteristics of the changes

(increase, decrease), we now included in this study the phase information and calculated additionally a phase angle map (PAM), which is derived from the angle component at stimulation frequency after performing the FFT. All computations except motion correction were performed using custom written software scripts in MATLAB (The MathWorks, Natick, MA). For a detailed flowchart, that shows the complete image processing chain for calculation of AAM and PAM, see Figure 2.

## 2.5 | Interpretation of phase angles derived from FFT

Since we used symmetric (equal length of rest and stimulation trials) stimulation patterns, we defined the zero-phase angle as the turning point between rest and stimulation trials and phase shifts were calculated in respect to this point. This has the advantage, that positive phase shifts are representing an increase of reflectance (Figure 3b, blue plot), whereas negative phase shifts are representing decreases of reflectance during the stimulation trials (Figure 3b, red plot).

With decreasing phase from 0 to  $-\pi$ , the time to the corresponding extreme value is moved towards the end of the stimulation trial, whereas with increasing phase from 0 to  $+\pi$ , the time of the extreme value is moved towards the beginning of the stimulation trial. The same applies to different length of the trials, as long as rest and stimulation have the same length. The reflectance change is connected through the tissue absorption inversely to the physiological component. An increased reflectance corresponds to a decrease of CBV or

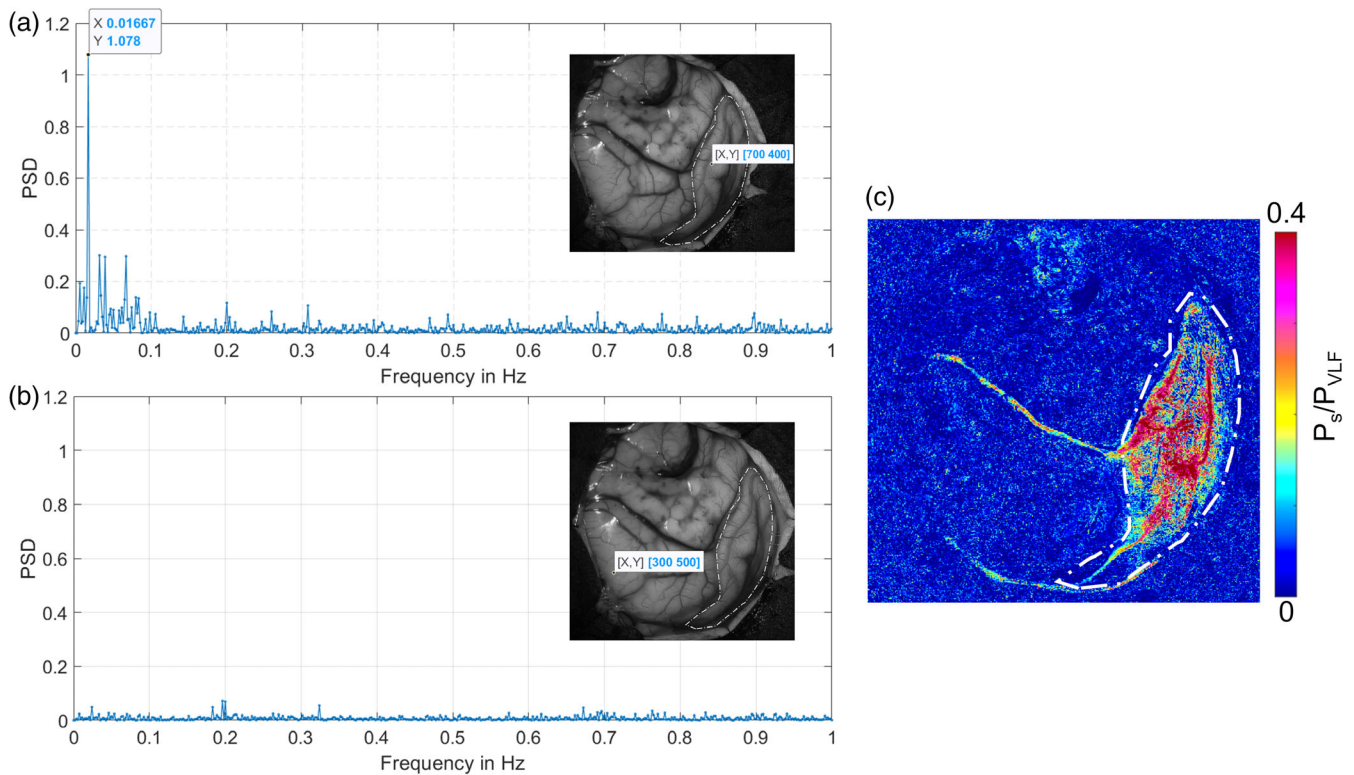


**FIGURE 1** Comparison of PSD for activated pixel (a) and nonactivated pixel (b) on primary sensory cortex (SI, dash-dotted line) of patient #10. The activation frequency of  $1/60$  (0.01667) Hz is clearly visible as distinct peak in (a), resulting from the used [30R – 30S] stimulation pattern used for electrical stimulation of the median nerve. The two-dimensional distribution of the ratio  $P_s/P_{VLF}$ , which is referred here as AAM, is shown in (c)

HbR (lower light absorption, due to lower concentration of CBV or HbR within tissue) and a decreased reflectance is corresponding to an increase of CBV or HbR (higher light absorption, due to higher concentration of CBV or HbR within tissue).

## 2.6 | Phase angle evaluation using polar histogram and image fusion of phase and amplitude information with whitelight image

We followed two different approaches for the visualization and comparison of the results. The first one is based on a polar histogram approach. A polar histogram is an objective measure for the phase angle distribution (PAD) at the cortical surface. To calculate the histograms, the trepanation as well as the activated gyrus were segmented in the whitelight images in the first step, taking the preoperative imaging data (MRI) into consideration. In patients that underwent sensory and tactile stimulation, the postcentral gyrus (SI) was segmented. In patients that were visually stimulated, the gyrus, on which the AAM showed activity, was segmented. During speech activation, multiple activations on different gyri were observed, therefore, the whole trepanned region was segmented as activated area. The resulting binary masks for trepanned area as well as for activated area were transferred afterwards to the AAM, which was thresholded with  $z_{\text{thresh}}$ , segmenting all pixels showing in the AAM an

activation level above mean activity level ( $\bar{A}_{\text{Trep}}$ ) plus standard deviation ( $\sigma_{\text{Trep}}$ ) within the trepanned area. The created binary mask of activation was applied on the phase image at stimulation frequency to calculate the polar histogram of only the activated area and the complete gyrus on which the activation is located. Binning was performed into groups separated  $\sim 0.1$  rad from each other (total of 62 groups ranging from  $-\pi$  to  $\pi$ ). Polar histogram bars are normalized to the total number of observations (bar height is representing percentage of total pixels). Due to the inversion between optical signal and physiological component (increase in CBV or HbR = decrease in reflectance and vice versa), the interval  $[0 \pi]$  corresponds to a decrease in the respective physiological component during the stimulation trial and  $[0 -\pi]$  corresponds with an increase during the stimulation trial. The time to minimum  $t_{\text{min}}$  increases towards zero phase angle, whereas the time to maximum  $t_{\text{max}}$  decreases towards zero phase angle, see also Figure 3. For the [30R – 30S] pattern,  $\pi$  would correspond to 30 s, whereas for the [15R – 15S] pattern,  $\pi$  would correspond to 15 s. To ease the interpretation, we use besides radian, also the time (in s) in the results section to quantify the phase angles. The calculation steps for the polar histogram are shown in Figure 4.

The second approach for data analysis used is the visualization of the combined information from AAM and PAM overlaid to the whitelight microscopy image of the intraoperative scene. It represents the direction of change at a glance and its spatial distribution on the

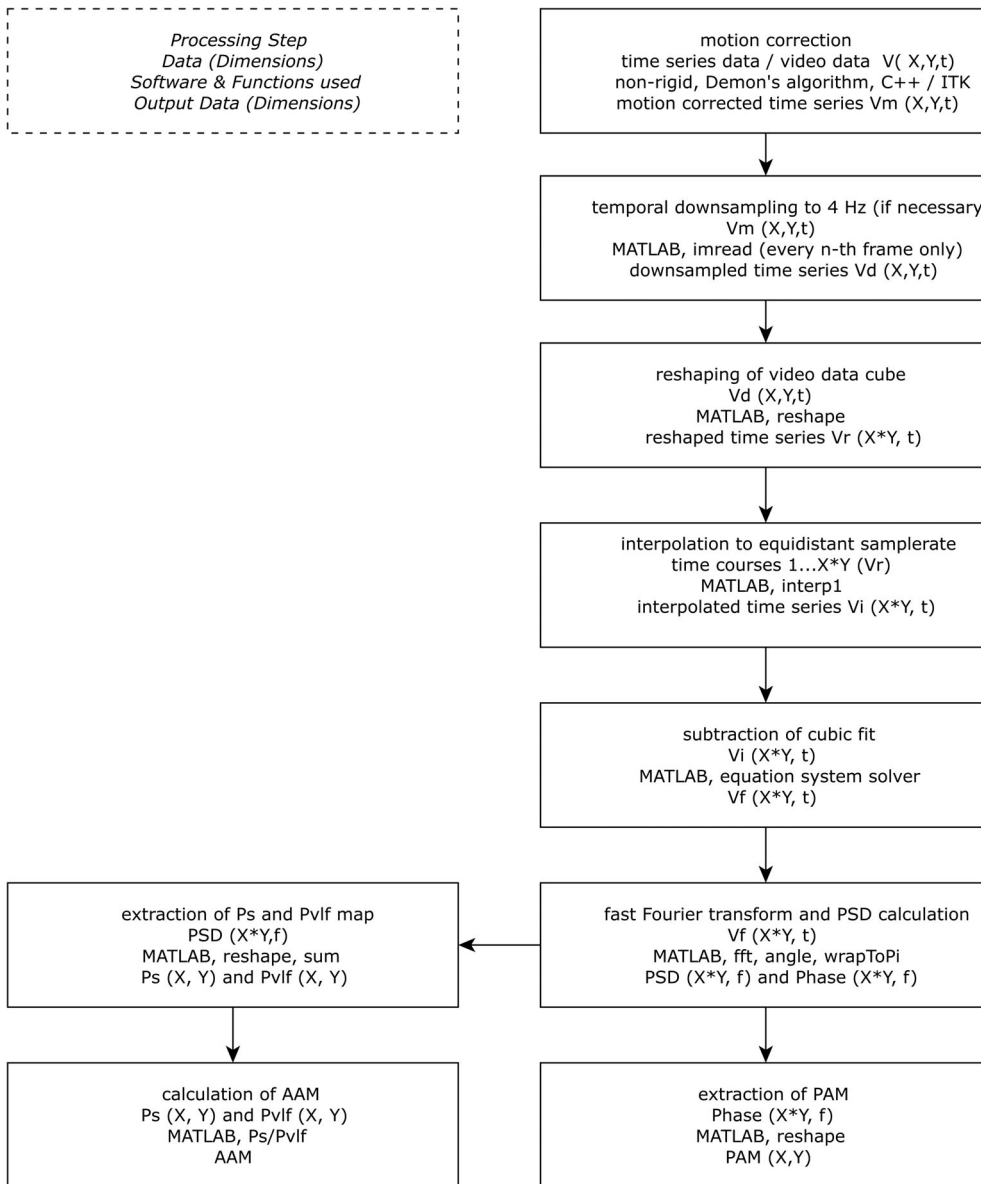


**FIGURE 2** Flowchart for image processing and calculation of AAM and PAM. The motion corrected and temporally downsampled image data is processed in MATLAB. Before performing FFT, timecourses are interpolated to equidistant samples to compensate variations in acquisition frame rate. Additionally, to remove constant component as well as to compensate for slow drifts in reflectance by desiccation of cortical surface, a cubic polynomial is fitted and subtracted from each timecourse. Power Spectral Density as well as phase angle of stimulation frequency component are calculated and then visualized within AAM, respectively, PAM

cortical surface. Therefore, we developed an image fusion approach in HSV color space, see Figure 5. The whitelight image (a), AAM (b), and PAM (c) are normalized to their maximum and merged in HSV color space, whereas the AAM is used as saturation, PAM as hue, and the whitelight image as value color plane. AAM and PAM are additionally smoothed using gauss filters with the kernel sizes  $\sigma_{AAM}$  and, respectively,  $\sigma_{PAM}$ . The resulting HSV image is converted back into RGB color space for visualization (d). The AAM is multiplied pixel-by-pixel with a scaling factor  $S$  that increases the extent of areas that are shown with color-coding in the resulting RGB image by increasing the actual normalized AAM pixel values within saturation plane (MATLAB is interpreting values of 1 with maximum saturation, values of 0 without any color saturation). It can be interpreted therefore as a threshold for the normalized activity level from which phase angle color-coding is performed in the output visualization. Due to the used image processing chain including smoothing utilizing gauss filtering, the maps are spatially averaged and therefore not as exact as the polar

histograms. Furthermore, the areas that are perceived as colored areas in this visualization are dependent of the scaling factor  $S$  of the AAM. An overview of the methodology can be found in Figure 5.

For inter-subject comparison of the different stimulation paradigms during electrical stimulation of median nerve (SI area), we calculated a spatial signal-to-noise ratio (SNR), which is defined as

$$SNR = \frac{n_{actSI}/n_{SI}}{n_{actSurr}/n_{surr}}$$

where  $n_{actSI}$  is the number of activated pixels (pixels within activity map with values  $> z_{thresh}$ , see Figure 1) on SI,  $n_{SI}$  is the number of total pixels within segmented SI area,  $n_{actSurr}$  is the number of activated pixels within the surrounding area (trepanation but not SI area), and  $n_{surr}$  is the total number of pixels within the surrounding area. The SNR is an indicator of how well the SI area can be distinguished from the surrounding tissue.

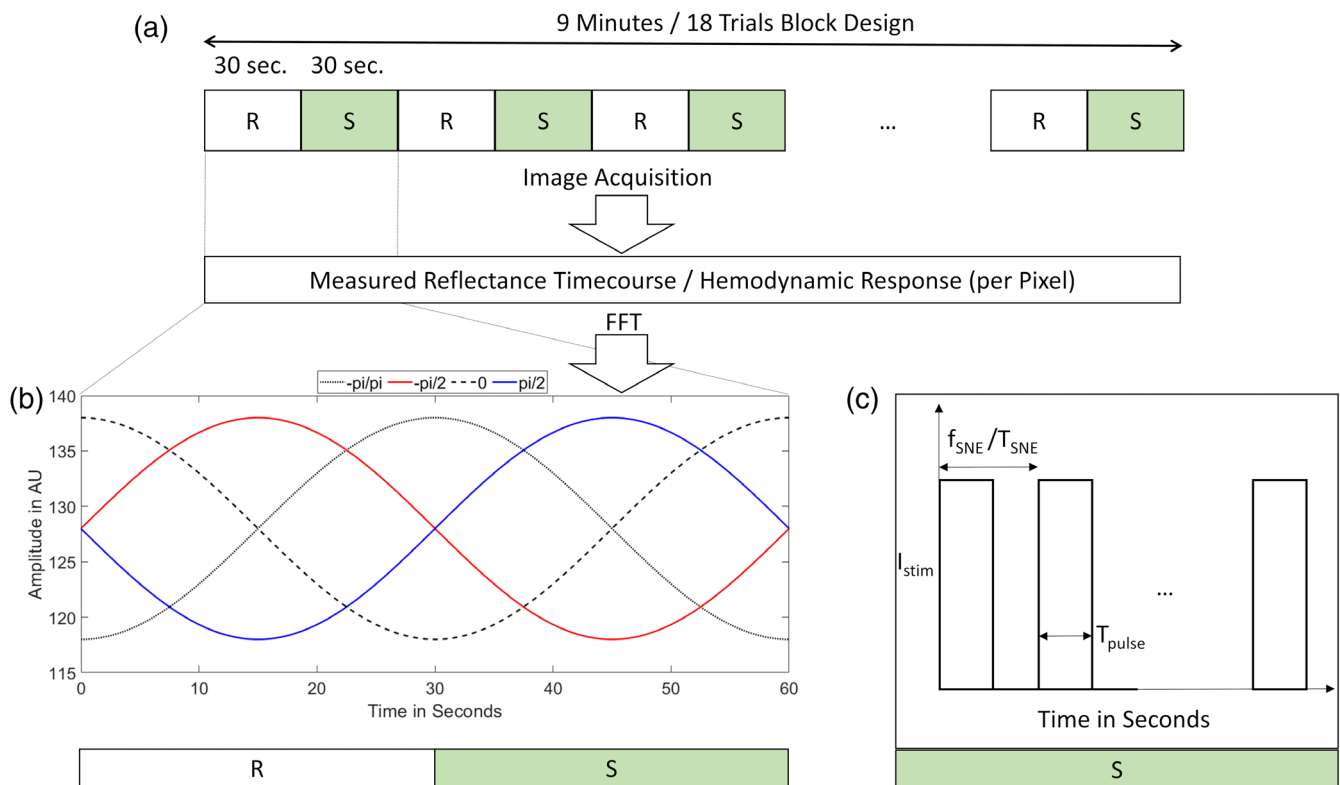


**FIGURE 3** (a) Schematic of [30R – 30S] stimulation pattern, consisting of 18 alternating rest and stimulation trials and starting with a rest trial. This results in an acquisition time of 9 min and corresponds to a stimulation frequency of 1/60 Hz (0.01667 Hz). The same design applies to the [15R – 15S] pattern, resulting in a total of 4.5 min of acquisition time and a stimulation frequency of 1/30 Hz (0.0334 Hz). The amplitude as well as the phase angles of those stimulation frequency components were derived for each pixel from the measured reflectance change timecourse using FFT approach. (b) Illustrates the definition of different phase angles for a synthetic sinusoidal 1/60 Hz component (mean graylevel 128, amplitude 10 gray level, typical 8-Bit digitalization range). The first two trials are shown. We defined the zero-phase as minimum of reflectance exactly between the two trials (here,  $t = 30$  s, dash line). A negative phase is therefore the correlate to a decrease of reflectance within the stimulation trial (illustrated here for phase angle of  $-\pi/2$ , red line), whereas a positive phase is the correlate to a maximum within stimulation trial (illustrated here for phase angle of  $\pi/2$ , blue line). (c) Shows the structure of a single stimulation trial. Within those trials, for example, electrical stimulation was performed with a stimulation frequency of  $f_{SNE}$  and a pulse duration of  $T_{pulse}$ . Those frequency components are compared to the block design stimulation component very high in their frequency and not part of the evaluation

### 3 | RESULTS

#### 3.1 | Electrical median nerve stimulation: Primary sensory cortex (SI)

The comparison of the PAD for different stimulation patterns and different observation wavelengths during electrical stimulation of the median nerve is shown in Figure 6. Comparing the PAD of  $\Delta$ CBV (568 nm signal, left, green) and  $\Delta$ HbR (600 nm/red channel signal, left, red) for electrical median nerve stimulation with [30R – 30S] pattern, a phase shift of about  $\pi$  (30 s) is visible, representing an increase of HbR during stimulation trials, whereas the local CBV is reduced during the stimulation compared towards rest trials (see also Figure 7 for averaged time courses of reflectance changes). The signals are inversely phased. The bin with the highest incidence is for the HbR group  $[-2.03-1.93]$  representing  $\sim 13\%$  of pixels. An amount of 57% of pixels is characterized in this group by phase angles between  $-\pi/2$  ( $t_{max} = -15$  s) and  $-2/3 \pi$  ( $t_{max} = -20$  s). The bin with the

highest incidence for the CBV group is  $[1.321.42]$  with  $\sim 13\%$  and the predominant phase angles ( $\sim 46\%$  of activated pixels) are here located between  $\pi/2$  ( $t_{min} = 15$  s) and  $\pi/3$  ( $t_{min} = 20$  s).

For [15R – 15S] pattern ( $\Delta$ CBV, right, cyan) the bin with the highest incidence is  $[0.71 0.81]$  with  $\sim 7\%$ , the predominant phase angles ( $\sim 33\%$  of activated pixels) are located between  $\pi/3$  ( $t_{min} = 10$  s) and  $\pi/6$  ( $t_{min} = 12.5$  s).

The detailed quantitative results for the intra-subject comparison of the different stimulation patterns using the activity map PSD ratio and SNR for the performance rating are part of Figure 8. In four out of five patients (patients #2, #3, #4, and #5), the [15R – 15S] pattern shows a higher median PSD ratio compared towards the [30R – 30S] pattern, whereas also in four out of five patients (patients #3, #4, #5, and #6) the SNR of the [30R – 30S] pattern is higher. This gives evidence, that there are less activated pixels that are not located on the SI area in comparison towards [15R – 15S] pattern. Figure 9 illustrates this fact in patient #3 and patient #4. Although the median PSD ratio on SI is for the [15R – 15S] pattern nearly equal or even higher



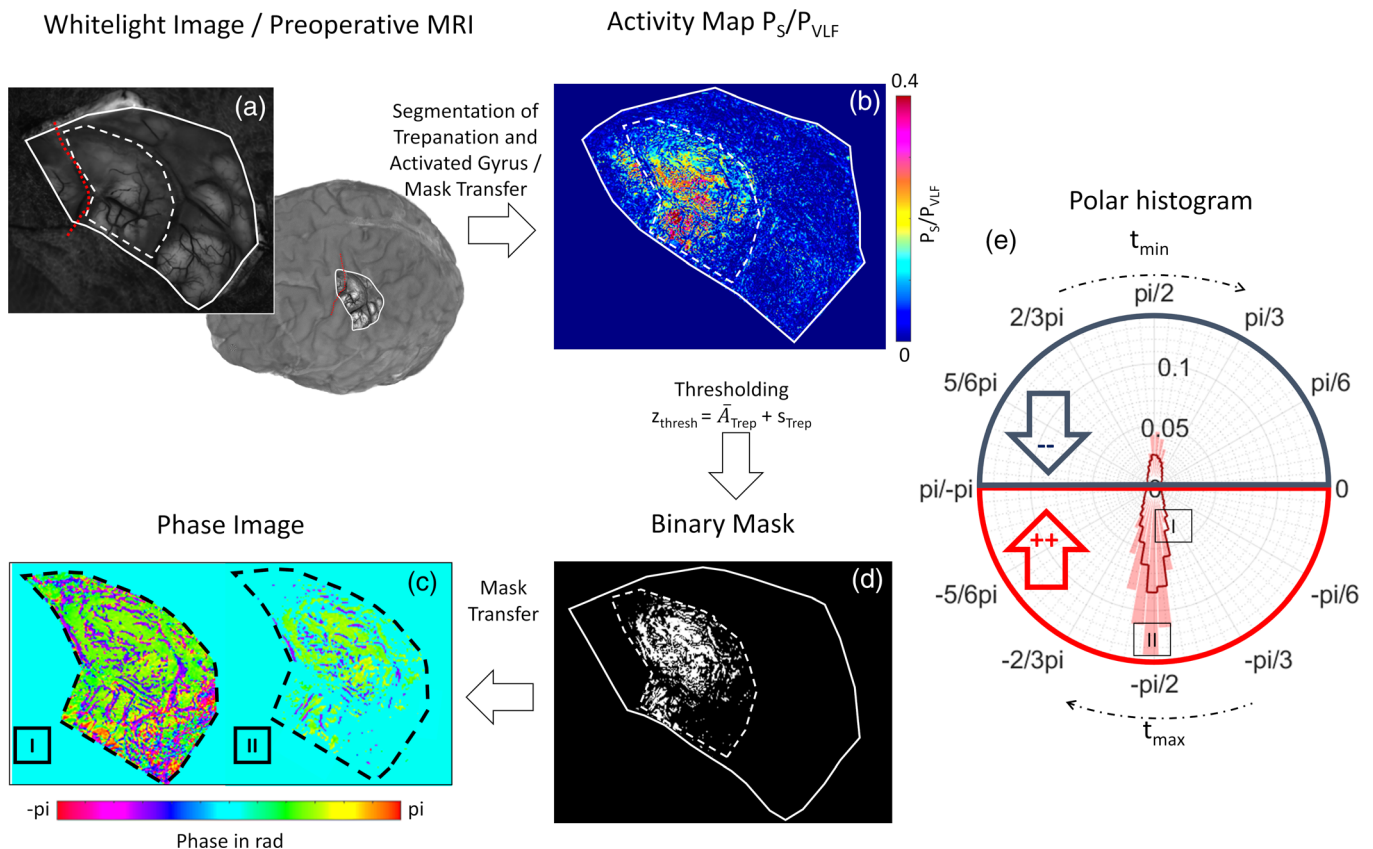


**FIGURE 4** Schematic of the polar histogram calculation. (a) Segmentation of the trepanation as well as the activated gyrus in the whitelight image. (b) Resulting binary masks for trepanned area as well as activated area overlaid to the AAM (c) thresholded ( $z_{\text{thresh}} = \bar{A}_{\text{Trep}} + s_{\text{Trep}}$ ) AAM. (d) Binary Mask of AAM overlaid to PAM at stimulation frequency. To calculate the polar histogram (e), the activated area (II, shaded) and the complete gyrus on which the activation is located (I, solid line, not filled) were used from (d). Arrows in (e) are in physiological notation regarding the direction of in-/decrease (not in reflectance measure)

in those patients, the SNR is worse, due to the activation of areas located on other gyri. Both patterns are resulting in positive phase angles and therefore in a decrease in CBV during stimulation trials, see also Figure 6.

### 3.2 | Tactile, visual, and speech stimulation

Comparison of the  $\Delta\text{CBV}$  PAD between electrical, tactile, visual, and speech activation ([30R – 30S] pattern, summarized over patients) is shown in Figure 10. The electrical stimulation of the median nerve reveals predominantly a positive phase angle ( $\sim 46\%$  of activated pixels) between  $\pi/2$  ( $t_{\text{min}} = 15$  s) and  $\pi/3$  ( $t_{\text{min}} = 20$  s), whereas tactile as well as visual stimulation responses are characterized by a predominantly negative phase angle ( $\sim 67\%$ , respectively,  $\sim 57\%$  of activated pixels) between  $-\pi/3$  ( $t_{\text{max}} = -10$  s) and  $-2/3\pi$  ( $t_{\text{max}} = -20$  s). Speech tasks are revealing a biphasic PAD with phase angles between  $2/3\pi$  ( $t_{\text{min}} = 10$  s) and  $\pi/3$  ( $t_{\text{min}} = 20$  s) within the positive half-plane ( $\sim 35\%$  of activated pixels) and between  $-\pi/3$  ( $t_{\text{max}} = -10$  s) and  $-2/3\pi$  ( $t_{\text{max}} = -20$  s) within the negative half-plane ( $\sim 37\%$  of activated pixels), respectively. Phase angle bins

of activated pixels with the highest incidence are as follows: [1.32, 1.42] with  $\sim 13\%$  for electrical stimulation,  $[-1.52, -1.62]$  with  $\sim 14\%$  for tactile stimulation,  $[-1.72, -1.82]$  with  $\sim 7\%$  for visual stimulation and  $[-1.62, -1.72]$  with  $\sim 7\%$  for speech tasks.

Representative maps of the phase angle for electrical, tactile, and visual stimulation, overlaid to the intraoperative scene are part of Figure 11. A decreased CBV (positive phase angle) on SI during the electrical stimulation trials of the median nerve is clearly visible, especially in the comparison towards tactile and visual stimulation paradigm, which lead to an increased CBV (negative phase angle). Speech tasks reveal delineated areas of increased CBV as well as areas with decreased CBV that are spatially closely located to each other. A detailed comparison of IOI results, fMRI, and intraoperative language site localization using Direct Cortical Stimulation (DCS) for patient #20 that performed the speech stimulation protocol can be found in Figure 12. The essential language site that was localized by DCS (marker #7) is characterized by a CBV decrease. Most of the other activations, visible in IOI, are characterized by a CBV increase (see Figure 12, part b). Representative time courses extracted from ROI1 with CBV increase and from ROI2 with CBV decrease are shown in part a of the figure.

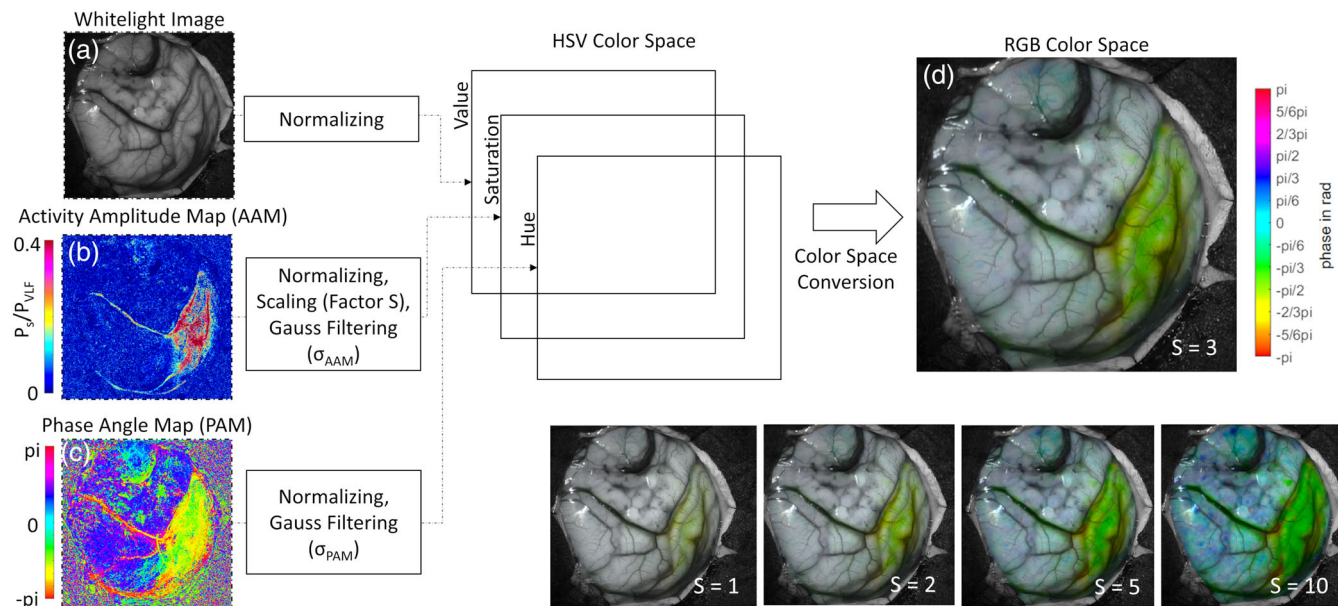


**FIGURE 5** Image processing chain for the pseudo colored visualization of PAM and AAM over the whitelight image of the intraoperative scene. Whitelight image (a), AAM (b), and PAM (c) are merged within HSV color space and the result is transferred back in RGB color space (d) for visualization. All images used in HSV color space were normalized to the interval [0 1]. AAM as well as PAM were smoothed used Gaussian filtering. The lower right part illustrates the influence of the scaling factor S on the final visualization

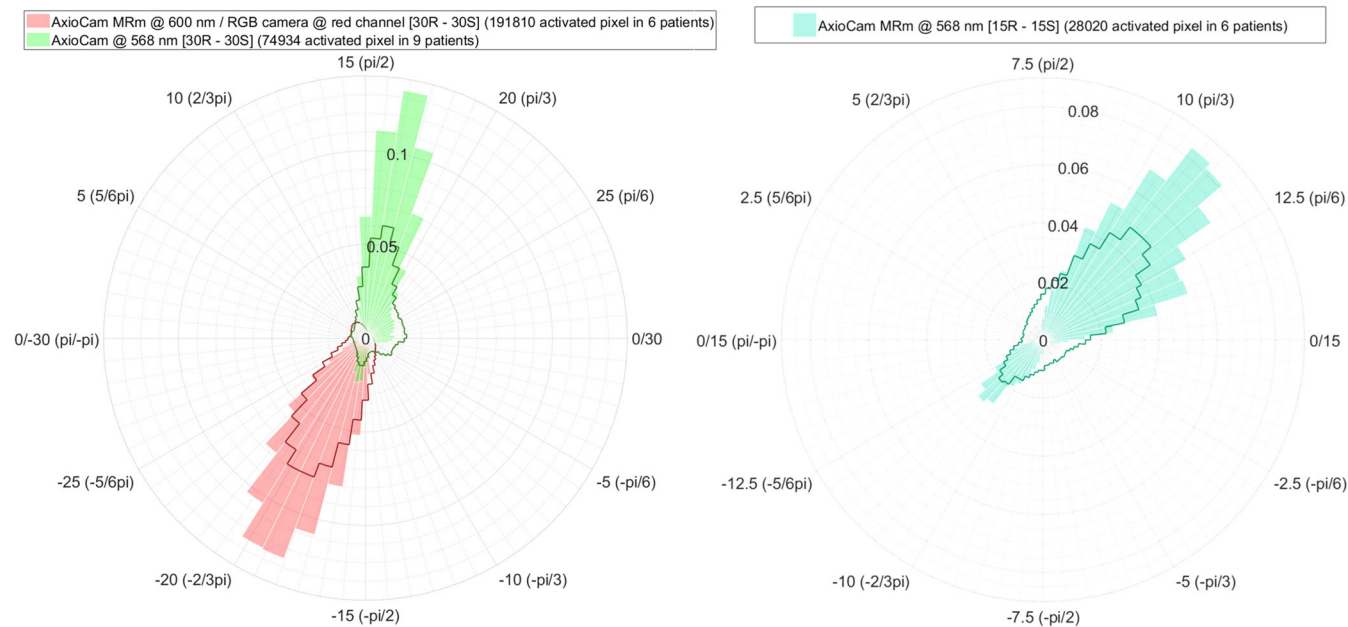


**FIGURE 6** Comparison of PAD summarized over patients for different stimulation patterns and observation wavelengths utilizing electrical stimulation of the median nerve. The resulting stimulation frequencies/oscillation times are 0.0167 Hz/60 s (pattern [30R – 30S], left side) and 0.0333 Hz/30 s (pattern [15R – 15S], right side). Percentage of activated pixels within positive/negative half-plane are as follows: 80%/20% (568 nm, [30R – 30S] pattern), 69%/31% (568 nm, [15R – 15S] pattern), and 8%/92% (600 nm/red channel, [30R – 30S] pattern). Polar axis is given in seconds (radian)

#### 4 | DISCUSSION

The results give evidence of a decrease in CBV together with an increase in HbR for electrical stimulation of the median nerve

(SI area). The maxima of both components during stimulation were reached, according to PAD, ~15–20 s after stimulation onset. Contrary to this, tactile activation of SI areas as well as visually evoked responses revealed areas with an increase in CBV

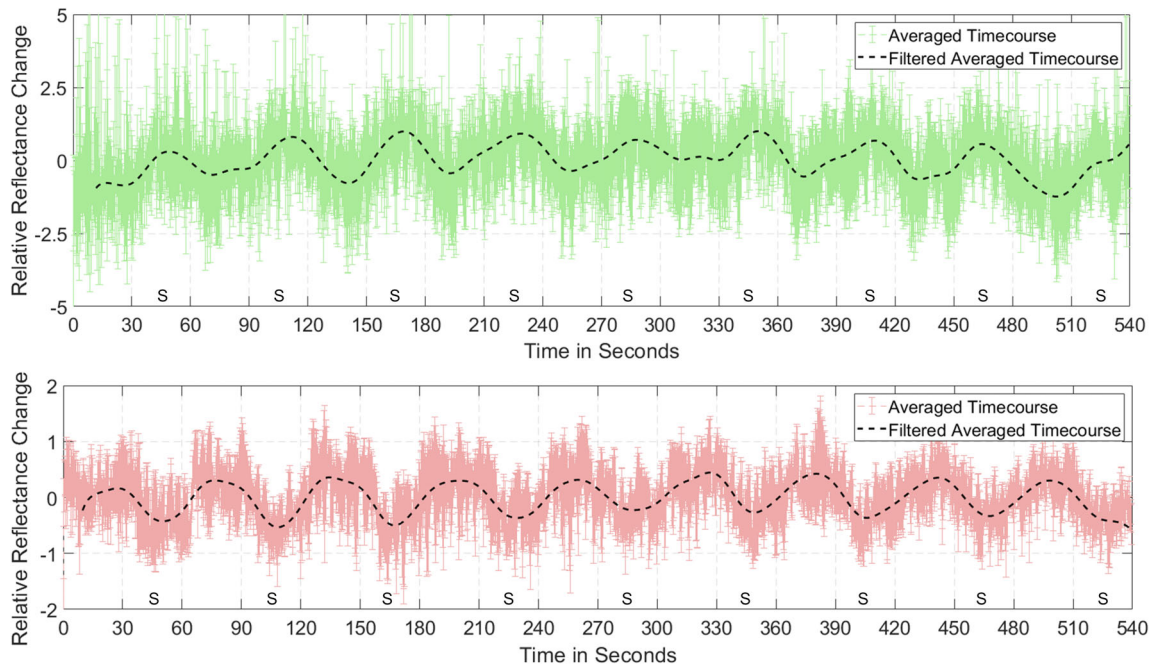


**FIGURE 7** Detrended and filtered timecourses of measured reflectance change on activated SI for the [30R – 30S] electrical stimulation of the median nerve. Stimulation trials are marked with “S.” Green: 568 nm reflectance change associated with CBV; Red: 600 nm/red channel reflectance change associated with HbR changes. Timecourses are averaged over patients (total of 9/6 patients, see also Figure 6 left for the corresponding PADs and Table 1). The dotted line is the filtered timecourse (zero-phase digital filter) of the cyclic stimulation component using the following filter design: FIR bandpass, cutoff frequencies: 0.01 Hz, 0.02 Hz). The inversely phased nature of both signals is clearly visible. *Note:* the timecourse processing/filtering is not linked to AAM or PAM calculations

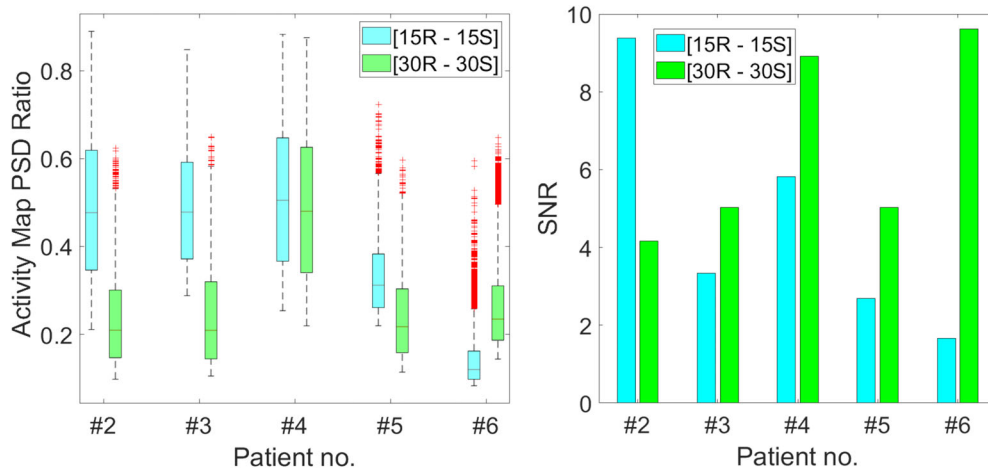


**FIGURE 8** Comparison of activity map PSD ratio (left) of activated pixels and SNR (right) for each patient in which both stimulation patterns were applied (patient #2, #3, #3, #4, #5, and #6). The median PSD ratio (Q1/Q3/n) for [15R – 15S] pattern are as follows: patient #2: 0.48 (0.35/0.62/7929), patient #3: 0.48 (0.37/0.59/4790), patient #4: 0.51 (0.37/0.65/7072), patient #5: 0.31 (0.26/0.38/2802), patient #6: 0.12 (0.10/0.16/5427). For [30R – 30S] pattern: patient #2: 0.21 (0.15/0.30/7249), patient #3: 0.21 (0.14/0.32/3224), patient #4: 0.48 (0.34/0.63/8864), patient #5: 0.22 (0.16/0.30/3180), patient #6: 0.24 (0.19/0.31/9825). The SNR of [15R – 15S]/[30R – 30S] pattern for the patients is: patient #2: 9.4/4.2, patient #3: 3.3/5.0, patient #4: 5.8/8.9, patient #5: 2.7/5.0, patient #6: 1.7/9.6

during the stimulation trials. Speech stimulation resulted in biphasic results within the language processing sites. Consecutively, we are discussing all relevant single aspects of our findings.

#### 4.1 | Origin of intrinsic signal

The optical signal for  $\Delta$ CBV originates from reflectance measure at 568 nm (10 nm FWHM) and is therefore due to same absorption of

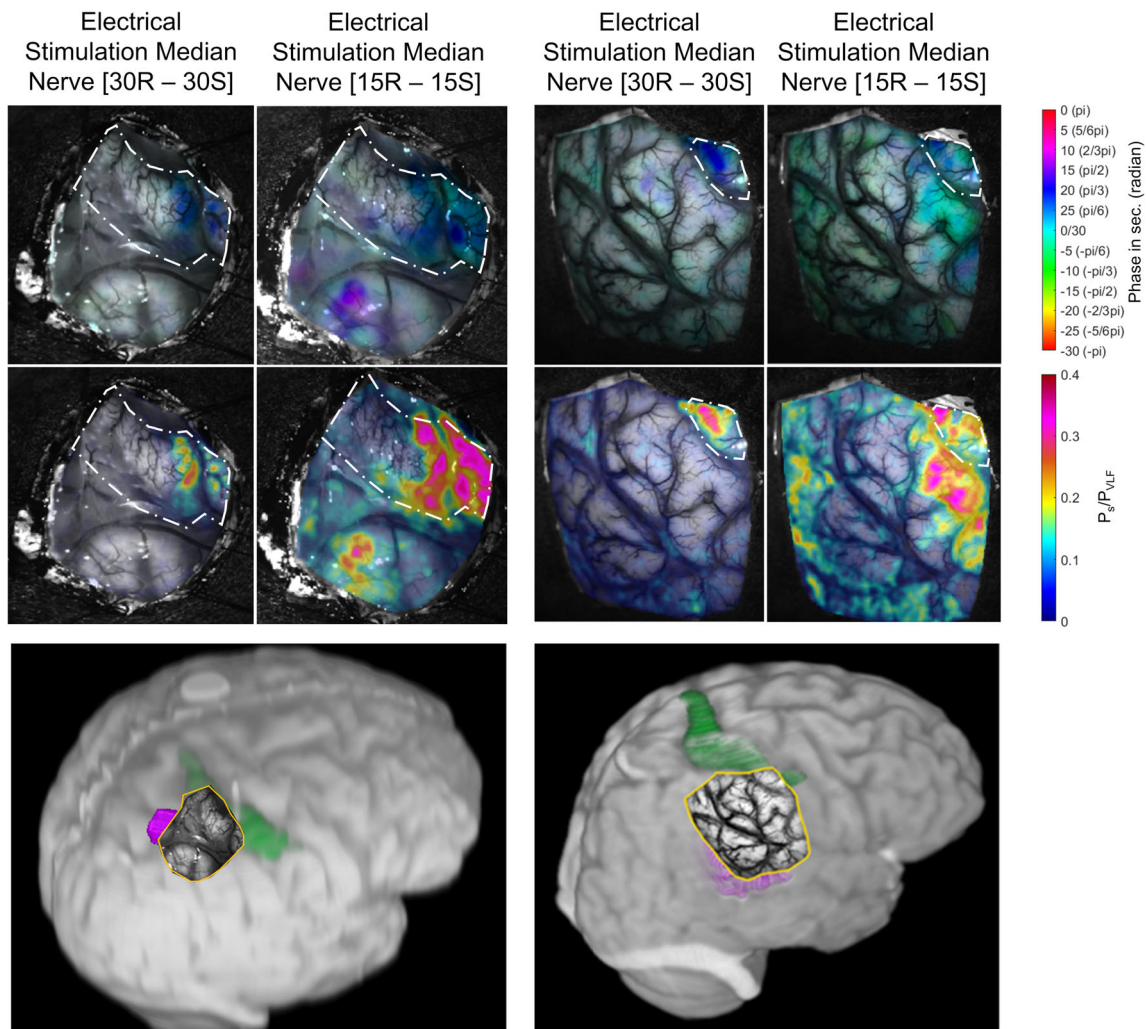


**FIGURE 9** Results of the different stimulations pattern in patient #3 (left) and patient #4 (right). The upper row shows the PAM, the middle row the AAM (postcentral gyrus marked with dash-dotted line), and the lower row the anatomical MRI, overlaid with the whitelight image of the intraoperative scene (trepanation borders in orange), segmented tumor volume (purple), and segmented postcentral gyrus (green)

HbR and HbO within this spectral range certainly dominated by changes of this component within the brain tissue. Some uncertainty arises for our HbR measure. The majority of the patients evaluated in respect to HbR changes were recorded using an RGB camera (3-Chip-CCD) with subsequent evaluation of the red channel (spectral response peak at 600 nm,  $\sim 50$  nm FWHM). Other physiological components (HbO, changes in scattering properties) may have contributed and contaminated this signal. Nevertheless, since the spectral response of the cameras red channel is not symmetric and characterized by a flatter slope towards NIR wavelengths, HbR should still be the dominating physiological component that is represented through the measurements. Additional evidence supporting this hypothesis is the fact that the results of patient measurements evaluated from those red channel data are consistent to the patient records with a narrowband 600 nm filter (10 nm FWHM, patient #3) and the fact that overall findings are consistent regarding the expected  $180^\circ$  phase shift of CBV and HbR. In general, the different hardware-setups that were used for the measurements, showed no significant differences

regarding the measured hemodynamic response, respectively, the regarding the different phase angles.

#### 4.2 | Comparison of IOI towards fMRI

IOI as well as fMRI are not able to provide a direct measurement for neural activity. Instead, hemodynamic effects, subsequent to the actual (electrical) activity are the signal source for both imaging modalities. CBF increases after neural activity lead to a decrease in local HbR that can be detected as BOLD response in fMRI or, with IOI, as a change in reflectance of the cortical surface within the spectral range  $\lambda > 600$  nm. In both modalities, the signal change is usually assessed in respect to a baseline condition. The common definition of “activation” is therefore an increase in BOLD response during stimulation, whereas the IOI correlate would be an increase in reflectance (both caused by a decrease of HbR). Hence, “deactivation” is defined as decrease of BOLD response/decrease of reflectance in respect to the

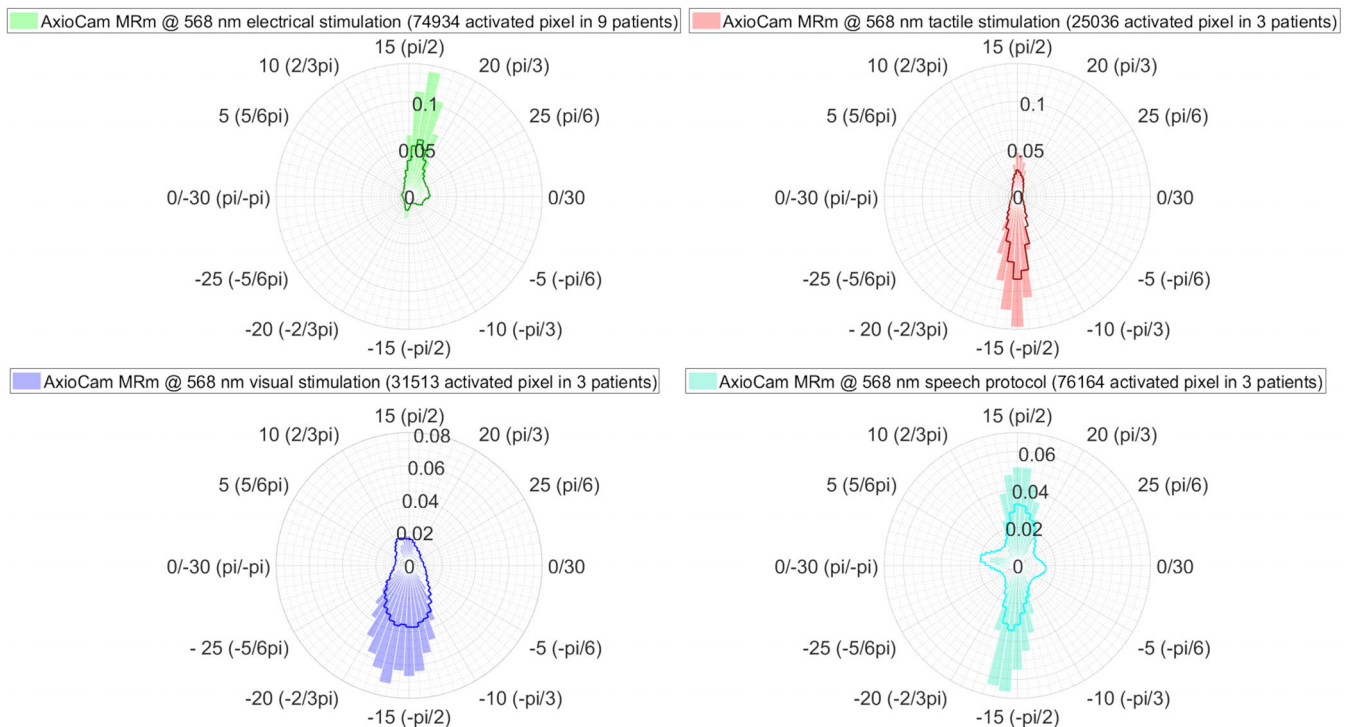


**FIGURE 10** PAD of 568 nm ( $\Delta$ CBV), following electrical (patients #1–#9), tactile (patients #8, #9, #16), visual (patients #17–#19), and speech activation (patients #20–#22), summarized over patients. Stimulation protocol is [30R – 30S], resulting in  $T_{\text{cycle}} = 2\pi = 60$  s. Solid lines represent the PAD on the activated gyrus, whereas the shaded histogram bars are representing the PAD of the activated pixels (see methodology section). Percentage of activated pixels within positive/negative half-plane are as follows: 80%/20% (electrical stimulation), 28%/72% (tactile stimulation), 20%/80% (visual stimulation), and 49%/51% (speech protocol). Polar axis is given in seconds (radian)

baseline condition during the stimulation trials (Uludag et al., 2004). Our IOI findings within spectral range of  $\lambda > 600$  nm can therefore be interpreted as correlate to the BOLD response, although there is evidence that both modalities may not exactly co-localize due to the fact that the optical signal may be contaminated by other signal sources like changes of light scattering properties within the tissue (Pouratian, Sicotte, et al., 2002b). Especially in our study, this might be the case due to the wide spectral response of the red channel (see also Section 4.1). Assuming that CBF and CBV are coupled to each other in neurovascular intact brain tissue, we interpret a CBV increase connected to an HbR decrease as an indicator for an also increased CBF and therefore for an activation of the area. The CBV decrease and HbR increase, observed in connection with the electrical stimulation of the median nerve, would therefore be the correlate to a NBR, which is in literature usually interpreted as neuronal/functional inhibition of the corresponding brain areas (Mullinger et al., 2014; Pasley, Inglis, & Freeman, 2007; Schäfer et al., 2012; Sten et al., 2017; Wade, 2002). Since we have for all other stimulation variants (visual, speech, tactile) only the measure of  $\Delta$ CBV, these results must be interpreted more carefully in respect to derived implications for fMRI results, since CBV does not have a direct correlate within BOLD response. Additionally, our findings are only valid for the very superficial layers of the cortex due to the low penetration depth of light within the visible range into the brain tissue. Therefore, it is possible, that fMRI still measures in larger and deeper volumes different or

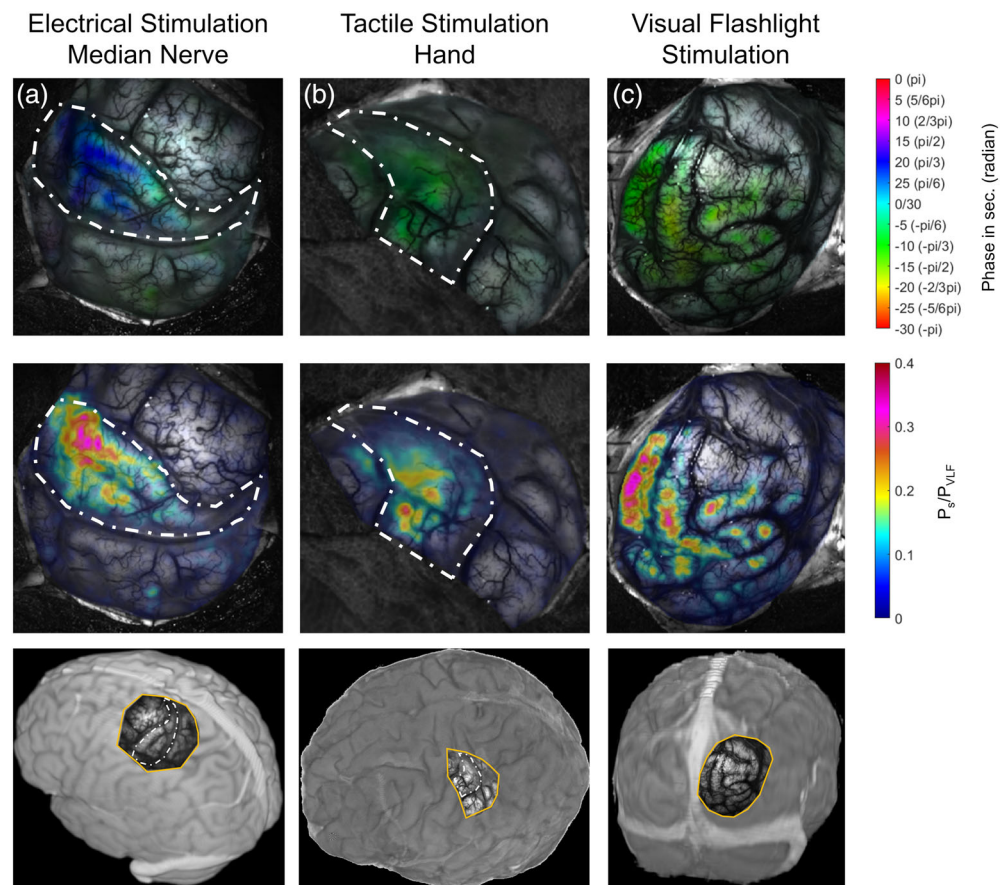
inverse effects than we observe directly on the surface using the IOI technique. Finally, the IOI measurements are limited to the exposed cortical region. Therefore, not the whole SI area can be imaged but only parts of it.

### 4.3 | Stimulus dependent hemodynamic response on primary sensory cortex (SI)

The phase angle evaluation is revealing a consistent and reproducible decrease of local CBV (reflectance measure at 568 nm) in SI during the stimulation trials whilst the patients were stimulated contralateral electrically on the median nerve. This behavior is contrary to the introductorily mentioned expected physiological hemodynamic response following cortical neural activation (CBF/CBV increase and HbR decrease [Hillman, 2014] and contrary to the CBV increase that we observed during tactile activation of SI area.

Evaluation of the reflectance changes acquired in the spectral range of the red channel/600 nm reveal additionally an increase of HbR during the stimulation trials, which would in fMRI terms be the correlate to an NBR (see also Section 4.2). The NBR is usually observed in SI either ipsilateral (Allison, Meador, Loring, Figueroa, & Wright, 2000; Kastrup et al., 2008; Klingner, Hasler, Brodoehl, & Witte, 2010) or in connection with painful stimuli (Bornhövd et al., 2002; Disbrow et al., 1998). Since our observations were all

**FIGURE 11** (a–c) Fusion of AAM, PAM, and whitelight image (upper row, see methodology section) of patient #6 (a), patient #16 (b), and patient #17 (c). The middle row shows the corresponding AAM. Dot-and-dashed line marks the postcentral gyrus (SI). The lower row shows the anatomical MRI for each patient, overlaid with the whitelight image of the intraoperative scene (trepanation borders in orange)



acquired from contralateral side, the results may give additional evidence of specific hemodynamic effects following cortical inhibition of the SI median nerve area due to processing of nociceptive stimuli. Apkarian et al. (1992) investigated nociceptive stimuli with SPECT and described a CBF decrease in SI subsequent to painful stimulation (cortical inhibition), whilst nonpainful stimuli led to increase in CBF. Our findings are in line with those results, since a reduction in CBF would plausibly explain, assuming an intact neurovascular coupling, a reduction of HbO in the corresponding area and an increase of HbR. Since CBV is linked to HbT ( $HbR + HbO$ ), and we have seen an HbR increase, the amplitude of the HbO decrease must be larger than the amplitude of the HbR increase. Otherwise, there would be no measure of a CBV decrease.

The cortical inhibition of SI area is visible using the [30R – 30S] stimulation pattern as well as the [15R – 15S] pattern. Contributing factors triggering this inhibitory hemodynamic response might be the high amplitude of the used stimulation current ( $I_{stim} = 20\text{ mA}$ ) and the prolonged stimulation trials, which would be in awake patients perceived as painful. In comparison to (Disbrow et al., 1998) who described pain thresholds for electrical stimuli delivered to the forefinger (surface electrodes) of  $I_{stim} = 20.8 \pm 10.4\text{ mA}$  in awake patients, we used in our study needle electrodes, placed directly in the nerve. Therefore, the pain threshold should be lower and nociceptive processing should have been triggered in SI even though patients were under general anesthesia. Nevertheless, there is no complete evidence, that the observed CBV decrease is solely due to the

nociceptive character of the stimulation and further investigations should exclude other, maybe causative, or at least contributing factors. A systematic variation of stimulation current amplitude as well as the use of surface electrodes for stimulation in further studies seem to be reasonable. Additionally, comparative measurements on a larger patient or subject cohort with other imaging modalities like fMRI are thinkable.

#### 4.4 | Spatial extent of SI activation using different stimulation patterns

Using the [15R – 15S] pattern for the median nerve stimulation, our results are revealing additional areas with inhibitory character (CBV decreases), located outside of the SI area, whereas the [30R – 30S] pattern leads to a spatially stronger localized CBV decrease, predominantly located only on SI area. Although the PSD ratio is in four out of five patients lower, the maps of the [30R – 30S] pattern are therefore better suited for the original task for which we initially optimized our IOI methodology: the identification of SI and other functional areas during surgical intervention. The origin of the additional regions with CBV decreases induced by using the [15R – 15S] pattern should be investigated in future research, technical factors, as well as physiological phenomena, should be taken into account. Going back to the assumption that our measured hemodynamic responses are inhibitory effects related to processing of painful stimuli, there is evidence in

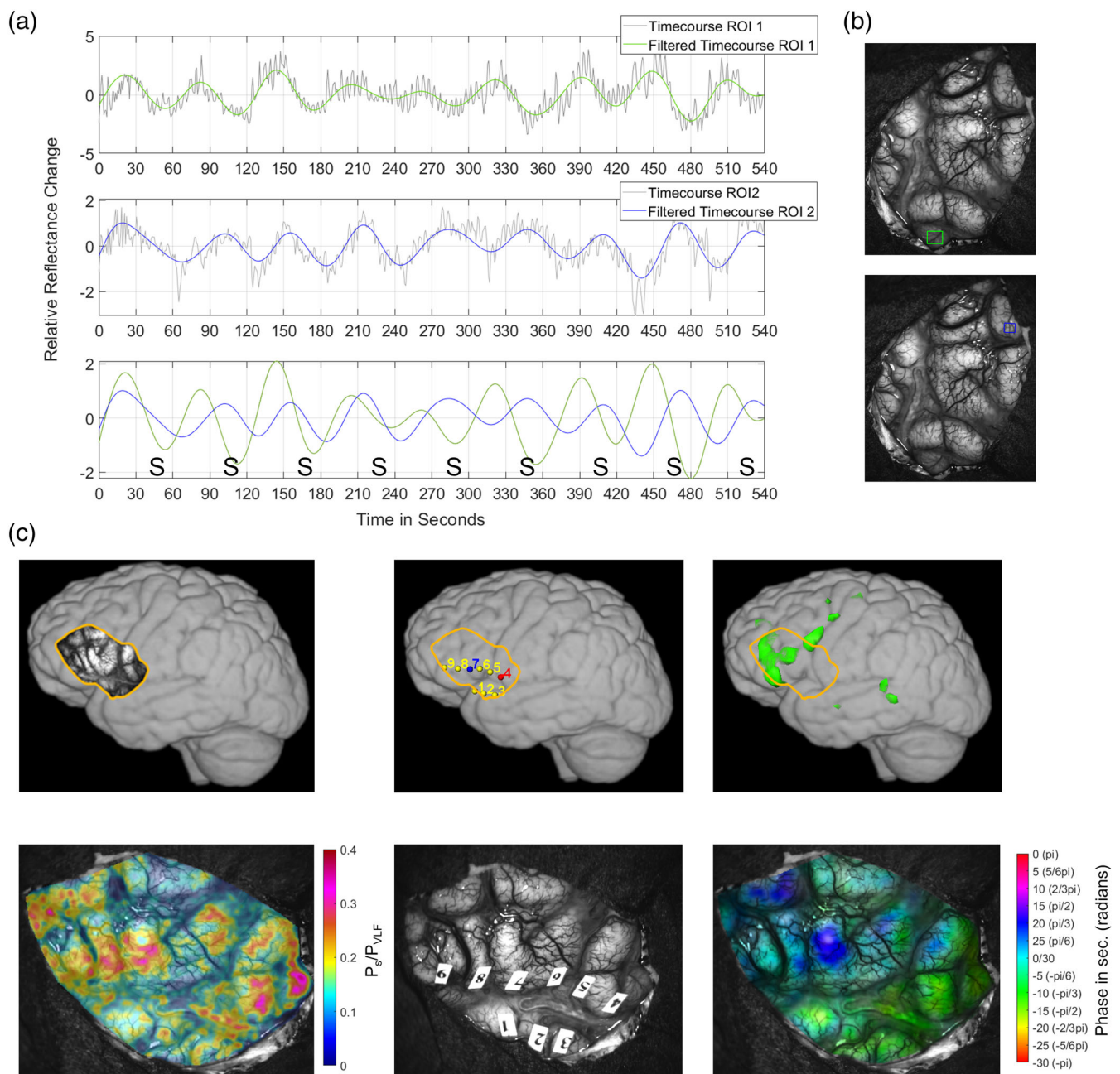


**FIGURE 12** (a) Timecourses of two different ROIs (b) extracted from areas with predominantly negative (green) and positive (blue; see additionally (c): right side, lower row) phase angle from patient #20 and the direct comparison of the detrended and filtered time courses. Filter design: FIR bandpass, cutoff frequencies: 0.01 Hz, 0.02 Hz. (b) Upper row from left to right: anatomical MRI with overlaid whitelight image; language localization using DCS: speech arrest at position #7, seizure at position #4 overlaid on anatomical MRI; preoperative fMRI results. Trepanation border is shown in orange. Lower row from left to right: AAM of [30R – 30S] speech stimulation, intraoperative view of DCS position markers, and PAM of [30R – 30S] speech stimulation (compare to ROI1 and ROI2 in a)

literature, that the role of SI in pain processing is foremost the stimulus intensity coding. In fMRI, the relationship between stimulation amplitude and BOLD response is described in general (ipsi- as well as contralateral) as a linear one (Bornhövd et al., 2002; Klingner et al., 2010). Bornhövd et al. (2002) observed besides this linear relation, a saturation plateau and a subsequent decrease in response. This decrease would be in line with the lower PSD ratio observed in the [30R – 30S] pattern compared to the [15R – 15S] pattern, whereas

the [30R – 30S] pattern is the correlate to the higher pain intensity. In respect to the pain intensity, Kong et al. (2010) observed in fMRI a greater spatial extent of the cortical regions that were deactivated when stimuli with lower pain intensity were applied. A higher pain intensity led inversely to a lower spatial extent. Our results support those findings assuming that the [15R – 15S] pattern is the correlate to the lower pain intensity. Nevertheless, in general the stimulus duration might also be contributing factor rather than the pain intensity only.

#### 4.5 | Comparison of PAD for different stimulation types

Comparing the PAD between the different stimuli variants, we found a 180° phase shift between electrical and tactile/visual stimulation. Additionally, we found a higher variability of the observed phase angles for visual stimulation compared to the other types. Speech areas revealed a clearly biphasic PAD with regional CBV decreases and increases closely located to each other. In fMRI language studies, observations of NBR (here CBV decrease/HbR increase) are also reported but the NBR is in comparison to the positive BOLD response still little investigated and up to now it is unclear if this is a side effect of vasomotor and mechanical variation, or if it is really connected to the activity (Binder, Swanson, Hammeke, & Sabsevitz, 2008; de Carli et al., 2007). Especially the spatial proximity (same or adjacent gyri) between activated and deactivated regions in our study is interesting and the fact, that essential language areas might have a different response than secondary language areas. The differentiation of generally activated areas in respect to the type of their hemodynamic response (inhibition/activation) might enable IOI in the future to separate between essential and secondary language areas, which is not possible up to now and as we found out in previous investigations, limits its application during awake surgery (Oelschlägel et al., 2020).

#### 4.6 | Study design and analysis limitations

The applied methodology for image data evaluation is based on the phase angle calculation at the stimulation frequency after performing an FFT. Therefore, we did not characterize, model, or observe individually the response to the stimulus resolved by each single trial. Nevertheless, this approach has the advantage that we do not have to make any assumptions about the expected hemodynamic responses except that they occur on the cortical surface with the same frequency as stimulation is performed. One weakness of the study design in general is the retrospective character and therefore due to unbalanced grouping of patient cohort the point, that a statistically robust investigation is not possible up to now. Another point, linked to this drawback, is the fact that CBV and HbR responses were obtained separately from different subjects and not simultaneously. Consequently, the findings should be verified in the future by using study designs with multi- or hyperspectral approaches for the synchronous acquisition of the wavelength bands corresponding with the different components (HbO, HbR, HbT). Quantitative approaches, using for example, a modification of the Beer–Lambert Law, are also thinkable.

#### 4.7 | Practical application of IOI

IOI is able to provide valuable information about the localization of functional areas and additionally about the character of the activation

during the neurosurgical intervention. It can be easily integrated into the OR due to the low additional hardware effort and the possibility to use the optical path of the surgical microscope. Nevertheless, some practical aspects during the application need to be considered. The method is susceptible to any variations of optical characteristics of the cortical surface. Therefore, it is best applied directly after craniotomy and before brain tissue is manipulated (e.g., before actual tumor resection starts). Bleeding that occurs on the cortical surface during measurements, is problematical since it affects the reflectance as well as specular reflections that occur during the measurements due to desiccation of the surface. According to our experience, it has proven to rinse thoroughly the surface before image acquisition is started. Additionally, the microscope used for image acquisition should be positioned in a flat angle towards the surface to minimize specular reflections. Light variations in the OR during the measurements must be avoided. Using the [30R – 30S] pattern, image acquisition takes 9 min, and the subsequent image analysis utilizing the FFT can be performed on a recent consumer computer within a few minutes. The computation time is predominantly dependent on the spatial resolution of the acquired images. IOI has the big advantage that the image data is acquired directly from the intraoperative scene. Therefore, it renders the occurring brain shift after craniotomy irrelevant and delivers precise information during the surgery. Using the microscope tracking of the neuronavigation system, an integration and fusion of IOI data with preoperatively acquired functional and anatomical data is possible in future application.

### 5 | CONCLUSIONS

Using an optimized IOI method, we analyzed cortical hemodynamic changes following electrical, tactile, visual and speech stimulation. In this study, we found a consistent and reproducible decrease of CBV (reflectance signal at 568 nm) in the SI area and an increase of HbR (reflectance signal >600 nm) during contralateral median nerve stimulation with needle electrodes. We interpret this effect as cortical inhibition of the stimulus processing area due to the nociceptive character of the stimulation. Using tactile stimulation protocol, CBV response was 180° phase shifted compared to the electrical stimulation. Additionally, for tactile, visual, and speech activation, differences in the corresponding phase angle distributions of the activated areas were identified. Summarizing the results, the specific stimulation protocol, the stimulation type as well as the stimulated function seem to have a nonnegligible impact on the observed phase angles and therefore on the provoked hemodynamic changes, their spatial localization, and their temporal characteristics. With the presented new methodology, optimization, and visualization of IOI, additional investigations of very specific questions about hemodynamic brain processes can be addressed. Especially future investigation of language processing seems, due to the clinical relevance, beneficial.

In the context of other brain imaging techniques, our findings are suggesting that models of hemodynamic brain functions have to be carefully applied, especially in patients with pathological brain



processes from which our results are obtained. Stimulation pattern, type, and parameter seem to influence the temporal behavior of triggered hemodynamics. Therefore, commonly used methods for identifying active areas based on hemodynamic response models combined with statistical evaluation might not be as accurate in every situation and patient as expected. Our work delivers an optimized methodology for getting valuable information about the hemodynamic response of CBV and HbR for different stimulation paradigms (visual, speech, tactile, and electrical), based on amplitude and especially phase angle maps evaluation by evaluating the optical reflectance signal. A quantitative multispectral approach would be the subsequent logical consequence for the future to separate the influence of methodological parameters on information about CBF, CBV, HbR, and HbO to describe neuronal activity and inhibition, hemodynamics, and general systemic control effects.

#### ACKNOWLEDGMENT

We would like to thank Andreas Schöppe, Anita Menschner, and Enrico Noback for their excellent technical assistance and support.

Open access funding enabled and organized by Projekt DEAL.

#### CONFLICT OF INTEREST

The authors declare no conflict of interest.

#### ETHICS APPROVAL AND PATIENT CONSENT STATEMENT

All measurements were approved by the ethics committee of the Technische Universität Dresden and informed consent was obtained from the patients before surgery.

#### DATA AVAILABILITY STATEMENT

Due to the retrospective character of the study, publication and sharing of the full intraoperative acquired raw image datasets were not part of the original study design. Since the data is related to the patients, image datasets will remain confidential.

#### ORCID

Martin Oelschlägel  <https://orcid.org/0000-0002-3776-3453>

#### REFERENCES

- Allison, J. D., Meador, K. J., Loring, D. W., Figueroa, R. E., & Wright, J. (2000). Functional MRI cerebral activation and deactivation during finger movement. *Neurology*, *54*, 135–135, 142.
- Ances, B. M., Leontiev, O., Perthen, J. E., Liang, C., Lansing, A. E., & Buxton, R. B. (2008). Regional differences in the coupling of cerebral blood flow and oxygen metabolism changes in response to activation: Implications for BOLD-fMRI. *NeuroImage*, *39*, 1510–1521.
- Apkarian, A. V., Stea, R. A., Manglos, S. H., Szeverenyi, N. M., King, R. B., & Thomas, F. D. (1992). Persistent pain inhibits contralateral somatosensory cortical activity in humans. *Neuroscience Letters*, *140*, 141–147.
- Arenth, P. M., Ricker, J. H., & Schultheis, M. T. (2007). Applications of functional near-infrared spectroscopy (fNIRS) to neurorehabilitation of cognitive disabilities. *The Clinical Neuropsychologist*, *21*, 38–57.
- Backes, W., Mess, W., van Kranen-Mastenbroek, V., & Reulen, J. (2000). Somatosensory cortex responses to median nerve stimulation: fMRI effects of current amplitude and selective attention. *Clinical Neurophysiology*, *111*, 1738–1744.
- Binder, J. R., Swanson, S. J., Hammeke, T. A., & Sabsevitz, D. S. (2008). A comparison of five fMRI protocols for mapping speech comprehension systems. *Epilepsia*, *49*, 1980–1997.
- Bornhövd, K., Quante, M., Glauche, V., Bromm, B., Weiller, C., & Büchel, C. (2002). Painful stimuli evoke different stimulus–response functions in the amygdala, prefrontal, insula and somatosensory cortex: A single-trial fMRI study. *Brain*, *125*, 1326–1336.
- Cannestra, A. F., Pouratian, N., Bookheimer, S. Y., Martin, N. A., Beckerand, D. P., & Toga, A. W. (2001). Temporal spatial differences observed by functional MRI and human intraoperative optical imaging. *Cerebral Cortex*, *11*, 773–782.
- Castellano, A., Cirillo, S., Bello, L., Riva, M., & Falini, A. (2017). Functional MRI for surgery of gliomas. *Current Treatment Options in Neurology*, *19*, 34.
- de Carli, D., Garreffa, G., Colonnese, C., Giulietti, G., Labruna, L., Briselli, E., ... Maraviglia, B. (2007). Identification of activated regions during a language task. *Magnetic Resonance Imaging*, *25*, 933–938.
- Disbrow, E., Buonocore, M., Antognini, J., Carstens, E., & Rowley, H. (1998). Somatosensory cortex: A comparison of the response to noxious thermal, mechanical, and electrical stimuli using functional magnetic resonance imaging. *Human Brain Mapping*, *6*, 150–159.
- Ferrari, M., Mottola, L., & Quaresima, V. (2004). Principles, techniques, and limitations of near infrared spectroscopy. *Canadian Journal of Applied Physiology*, *29*, 463–487.
- Goense, J., Merkle, H., & Logothetis, N. K. (2012). High-resolution fMRI reveals laminar differences in neurovascular coupling between positive and negative BOLD responses. *Neuron*, *76*, 629–639.
- Hadjiabadi, D. H., Pung, L., Zhang, J., Ward, B. D., Lim, W. T., Kalavar, M., ... Pathak, A. P. (2018). Brain tumors disrupt the resting-state connectome. *NeuroImage: Clinical*, *18*, 279–289.
- Haglund, M. M., Ojemann, G. A., & Hochman, D. W. (1992). Optical imaging of epileptiform and functional activity in human cerebral cortex. *Nature*, *358*, 668–671.
- Hillman, E. M. (2014). Coupling mechanism and significance of the BOLD signal: A status report. *Annual Review of Neuroscience*, *37*, 161–181.
- Huber, L., Goense, J., Kennerley, A. J., Ivanov, D., Krieger, S. N., Lepsien, J., ... Möller, H. E. (2014). Investigation of the neurovascular coupling in positive and negative BOLD responses in human brain at 7 T. *NeuroImage*, *97*, 349–362.
- Huppert, T. J., Allen, M. S., Diamond, S. G., & Boas, D. A. (2009). Estimating cerebral oxygen metabolism from fMRI with a dynamic multicompartment Windkessel model. *Human Brain Mapping*, *30*, 1548–1567.
- Kapsalakis, I. Z., Kapsalaki, E. Z., Gotsis, E. D., Verganelakis, D., Toulas, P., Hadjigeorgiou, G., ... Fountas, K. N. (2012). Preoperative evaluation with FMRI of patients with intracranial gliomas. *Radiology Research and Practice*, *2012*, 1–17.
- Kastrup, A., Baudewig, J., Schnaudigel, S., Huonker, R., Becker, L., Sohns, J. M., ... Witte, O. W. (2008). Behavioral correlates of negative BOLD signal changes in the primary somatosensory cortex. *NeuroImage*, *41*, 1364–1371.
- Klingner, C. M., Hasler, C., Brodoehl, S., & Witte, O. W. (2010). Dependence of the negative BOLD response on somatosensory stimulus intensity. *NeuroImage*, *53*, 189–195.
- Kong, J., Loggia, M. L., Zyloney, C., Tu, P., LaViolette, P., & Gollub, R. L. (2010). Exploring the brain in pain: Activations, deactivations and their relation. *Pain*, *148*, 257–267.
- Ma, Y., Shaik, M. A., Kim, S. H., Kozberg, M. G., Thibodeaux, D. N., Zhao, H. T., ... Hillman, E. M. C. (2016). Wide-field optical mapping of neural activity and brain haemodynamics: Considerations and novel approaches. *Philosophical Transactions of the Royal Society B: Biological Sciences*, *371*, 20150360.

- Macé, E., Montaldo, G., Cohen, I., Baulac, M., Fink, M., & Tanter, M. (2011). Functional ultrasound imaging of the brain. *Nature Methods*, 8, 662–664.
- Mace, E., Montaldo, G., Osmanski, B. F., Cohen, I., Fink, M., & Tanter, M. (2013). Functional ultrasound imaging of the brain: Theory and basic principles. *IEEE Transactions on Ultrasonics, Ferroelectrics, and Frequency Control*, 60, 492–506.
- Meyer, T., Sobottka, S. B., Kirsch, M., Schackert, G., Steinmeier, R., Koch, E., & Morgenstern, U. (2013). Intraoperative optical imaging of functional brain areas for improved image-guided surgery. *Biomedizinische Technik/Biomedical Engineering*, 58, 225–236.
- Mikdashi, J. A. (2016). Altered functional neuronal activity in neuropsychiatric lupus: A systematic review of the fMRI investigations. *Seminars in Arthritis and Rheumatism*, 45, 455–462.
- Morone, K. A., Neimat, J. S., Roe, A. W., & Friedman, R. M. (2017). Review of functional and clinical relevance of intrinsic signal optical imaging in human brain mapping. *Neurophotonics*, 4, 031220.
- Mullinger, K. J., Mayhew, S. D., Bagshaw, A. P., Bowtell, R., & Francis, S. T. (2014). Evidence that the negative BOLD response is neuronal in origin: A simultaneous EEG–BOLD–CBF study in humans. *NeuroImage*, 94, 263–274.
- Oelschlägel, M., Meyer, T., Morgenstern, U., Wahl, H., Gerber, J., Reiß, G., ... Sobottka, S. B. (2020). Mapping of language and motor function during awake neurosurgery with intraoperative optical imaging. *Neurosurgical Focus*, 48, E3.
- Oelschlägel, M., Meyer, T., Wahl, H., Sobottka, S. B., Kirsch, M., Schackert, G., & Morgenstern, U. (2013). Evaluation of intraoperative optical imaging analysis methods by phantom and patient measurements. *Biomedizinische Technik/Biomedical Engineering*, 58, 257–267.
- Oelschlägel, M., Meyer, T., Schackert, G., Kirsch, M., Sobottka, S. B., & Morgenstern, U. (2018). Intraoperative optical imaging of metabolic changes after direct cortical stimulation: a clinical tool for guidance during tumor resection? *Biomedical Engineering/Biomedizinische Technik*, 63(5), 587–594.
- Parkes, L. M., Fries, P., Kerskens, C. M., & Norris, D. G. (2004). Reduced BOLD response to periodic visual stimulation. *NeuroImage*, 21, 236–243.
- Pasley, B. N., Inglis, B. A., & Freeman, R. D. (2007). Analysis of oxygen metabolism implies a neural origin for the negative BOLD response in human visual cortex. *NeuroImage*, 36, 269–276.
- Pouratian, N., Cannestra, A. F., Martin, N. A., & Toga, A. W. (2002a). Intraoperative optical intrinsic signal imaging: A clinical tool for functional brain mapping. *Neurosurgical Focus*, 13, 1–9.
- Pouratian, N., Sicotte, N., Rex, D., Martin, N. A., Becker, D., Cannestra, A. F., & Toga, A. W. (2002b). Spatial/temporal correlation of BOLD and optical intrinsic signals in humans. *Magnetic Resonance in Medicine: An Official Journal of the International Society for Magnetic Resonance in Medicine*, 47, 766–776.
- Prakash, N., Uhlemann, F., Sheth, S. A., Bookheimer, S., Martin, N., & Toga, A. W. (2009). Current trends in intraoperative optical imaging for functional brain mapping and delineation of lesions of language cortex. *NeuroImage*, 47, T116–T126.
- Robinson, P. A., Drysdale, P. M., van der Merwe, H., Kyriakou, E., Rigozzi, M. K., Germanoska, B., & Rennie, C. J. (2006). BOLD responses to stimuli: Dependence on frequency, stimulus form, amplitude, and repetition rate. *NeuroImage*, 31, 585–599.
- Sanai, N., & Berger, M. S. (2008). Glioma extent of resection and its impact on patient outcome. *Neurosurgery*, 62, 753–766.
- Sato, K., Nariai, T., Sasaki, S., Yazawa, I., Mochida, H., Miyakawa, N., ... Ohno, K. (2002). Intraoperative intrinsic optical imaging of neuronal activity from subdivisions of the human primary somatosensory cortex. *Cerebral Cortex*, 12, 269–280.
- Sato, K., Nariai, T., Tanaka, Y., Maehara, T., Miyakawa, N., Sasaki, S., ... Ohno, K. (2005). Functional representation of the finger and face in the human somatosensory cortex: Intraoperative intrinsic optical imaging. *NeuroImage*, 25, 1292–1301.
- Schäfer, K., Blankenburg, F., Kupers, R., Grüner, J. M., Law, I., Lauritzen, M., & Larsson, H. B. W. (2012). Negative BOLD signal changes in ipsilateral primary somatosensory cortex are associated with perfusion decreases and behavioral evidence for functional inhibition. *NeuroImage*, 59, 3119–3127.
- Senft, C., Bink, A., Franz, K., Vatter, H., Gasser, T., & Seifert, V. (2011). Intraoperative MRI guidance and extent of resection in glioma surgery: A randomised, controlled trial. *The Lancet Oncology*, 12, 997–1003.
- Silva, M. A., See, A. P., Essayed, W. I., Golby, A. J., & Tie, Y. (2018). Challenges and techniques for presurgical brain mapping with functional MRI. *NeuroImage: Clinical*, 17, 794–803.
- Sobottka, S. B., Meyer, T., Kirsch, M., Koch, E., Steinmeier, R., Morgenstern, U., & Schackert, G. (2013a). Intraoperative optical imaging of intrinsic signals: A reliable method for visualizing stimulated functional brain areas during surgery: Clinical article. *Journal of Neurosurgery*, 119, 853–863.
- Sobottka, S. B., Meyer, T., Kirsch, M., Reiss, G., Koch, E., Morgenstern, U., & Schackert, G. (2013b). Assessment of visual function during brain surgery near the visual cortex by intraoperative optical imaging. *Biomedizinische Technik/Biomedical Engineering*, 58, 249–256.
- Sotero, R. C., & Trujillo-Barreto, N. J. (2008). Biophysical model for integrating neuronal activity, EEG, fMRI and metabolism. *NeuroImage*, 39, 290–309.
- Stefanovic, B., Warnking, J. M., & Pike, G. B. (2004). Hemodynamic and metabolic responses to neuronal inhibition. *NeuroImage*, 22, 771–778.
- Sten, S., Lundengård, K., Witt, S. T., Cedersund, G., Elinder, F., & Engström, M. (2017). Neural inhibition can explain negative BOLD responses: A mechanistic modelling and fMRI study. *NeuroImage*, 158, 219–231.
- Stummer, W., Reulen, H. J., Meinel, T., Pichlmeier, U., Schumacher, W., Tonn, J. C., ... ALA-Glioma Study Group. (2008). Extent of resection and survival in glioblastoma multiforme: Identification of and adjustment for bias. *Neurosurgery*, 62, 564–576.
- Suh, M., Bahar, S., Mehta, A. D., & Schwartz, T. H. (2006). Blood volume and hemoglobin oxygenation response following electrical stimulation of human cortex. *NeuroImage*, 31, 66–75.
- Tal, Z., Geva, R., & Amedi, A. (2017). Positive and negative somatotopic BOLD responses in contralateral versus ipsilateral penfield homunculus. *Cerebral Cortex*, 27, 962–980.
- Thirion, J.-P. (1998). Image matching as a diffusion process: An analogy with Maxwell's demons. *Medical Image Analysis*, 2, 243–260.
- Uludağ, K., Dubowitz, D. J., Yoder, E. J., Restom, K., Liu, T. T., & Buxton, R. B. (2004). Coupling of cerebral blood flow and oxygen consumption during physiological activation and deactivation measured with fMRI. *NeuroImage*, 23, 148–155.
- van den Heuvel, M. P., & Pol, H. E. H. (2010). Exploring the brain network: A review on resting-state fMRI functional connectivity. *European Neuropsychopharmacology*, 20, 519–534.
- Villringer, A., Planck, J., Hock, C., Schleinkofer, L., & Dirnagl, U. (1993). Near infrared spectroscopy (NIRS): A new tool to study hemodynamic changes during activation of brain function in human adults. *Neuroscience Letters*, 154, 101–104.
- Wade, A. R. (2002). The negative BOLD signal unmasked. *Neuron*, 36, 993–995.
- Wilson, R., Thomas, A., & Mayhew, S. D. (2020). Spatially congruent negative BOLD responses to different stimuli do not summate in visual cortex. *NeuroImage*, 218, 116891.

**How to cite this article:** Oelschlägel, M., Polanski, W. H., Morgenstern, U., Steiner, G., Kirsch, M., Koch, E., Schackert, G., & Sobottka, S. B. (2022). Characterization of cortical hemodynamic changes following sensory, visual, and speech activation by intraoperative optical imaging utilizing phase-based evaluation methods. *Human Brain Mapping*, 43(2), 598–615. <https://doi.org/10.1002/hbm.25674>